

A BASELINE EVALUATION OF THE CYTOTOXICITY OF  
GOLD NANOPARTICLES IN DIFFERENT TYPES OF  
MAMMALIAN CELLS FOR FUTURE RADIOSENSITIZATION  
STUDIES

BY

SHANA DE BRUYN

2020



UNIVERSITY *of the*  
WESTERN CAPE

**A BASELINE EVALUATION OF THE CYTOTOXICITY OF GOLD  
NANOPARTICLES IN DIFFERENT TYPES OF MAMMALIAN CELLS  
FOR FUTURE RADIOSENSITIZATION STUDIES**

by

**SHANA DE BRUYN**

**3438423**

**SUBMITTED IN PARTIAL FULFILMENT FOR THE DEGREE  
*MAGISTER SCIENTIAE***

**(NANOSCIENCE)**

*in the*

**FACULTY OF NATURAL SCIENCE, DEPARTMENT OF MEDICAL  
BIOSCIENCE**

at the

**UNIVERSITY OF THE WESTERN CAPE**

**BELLVILLE**

**SOUTH AFRICA**

**SUPERVISOR:** Prof. M. de Kock

**CO-SUPERVISOR:** Dr. C. Vandevoorde

**DECEMBER 2020**

## DECLARATION

---

I, the undersigned, hereby declare that the work contained in this thesis titled **A Baseline Evaluation of the Cytotoxicity of Gold Nanoparticles in Different Types of Mammalian Cells for Future Radiosensitization Studies** is my own work and has not been previously submitted for any degree or assessment at any university.

All sources and material that I have utilized or quoted have been indicated and acknowledged by means of complete references.

---

Shana De Bruyn

---

Date



## ACKNOWLEDGMENTS

---

Thank you to the heavenly father for making this possible, because through him all is possible. The Lord has blessed me abundantly, I want to say thank you for the strength and patience he has bestowed upon me. This has been a trying year and I would not have been able to endure half of it if not for the prayers. God gives us what we need and not what we want and I am eternally grateful for everything he has blessed and allowed in my life. I pray that his mercies and blessing remain with me all my days.

I wish to extend my heartfelt gratitude to the following institutions and individuals for their incredible contributions to this research paper:

**Edith Appollis and Broderick De Bruyn (Parents):** I cannot express my thankfulness enough for everything you have done and sacrificed for me. I want to say Thank you for the support, love and constant motivation. Through the laughs, tears, failures and success you have been my foundation and I am eternally grateful. Thank for allowing me to grow and always being by my side.

**Bronwin Orr (Fiancé):** My main motivator and the person that has been there through the ups and downs of this research, thank you so much for your support and unconditional love. Your patience and advice I will cherish always, I am so grateful to have you in my life.

**Professor Maryna De Dock (Supervisor):** Thank you so much for all the guidance, support and lessons you have taught me since my Honours year. The skills and life lessons I have gained under your supervision is something I will cherish and utilize in my future endeavours. Thank you for the encouraging words which have allowed me to grow and become the student I am. You are truly an amazing, fun loving person and it has be a privilege to be your student.

**Dr. Charlot Vandevoorde (Co-Supervisor):** I would like to thank you for always being there and always providing encouragement. Thank you for the rapid responses and valuable advice throughout this trying year. You really are an outstanding person and one of the friendliest people I have ever come across. You are truly an inspiration to young woman in science.

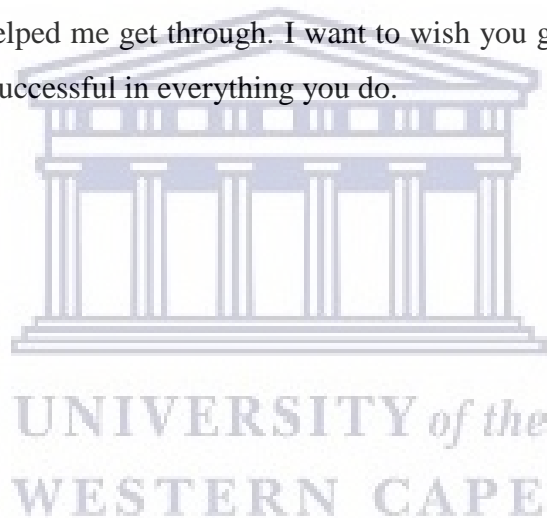
**UWC (Institution and Peers):** Thank you to all the friends and acquaintances for the help, advice and brilliant knowledge shared with me. Collaborations and extending a helping hand was definitely a trait that was ever present in the MBS department. To UWC thank you for providing a productive and safe working environment.

**iThemba Labs:** I would like to extend my thanks to iThemba labs and the staff for the guidance and providing an exceptional educational environment.

**Amelia Jansen Van Vuuren:** The honours student who has been a major help and vital contribution to this study, thank you for the countless hours invested into this project, the support, laughs, lunches and late days. I am grateful for the friendship we have developed over this short yet intense year. You are amazing.

**Mrs. Valencia Jamali and Mrs. Chyril Abrahams:** Nanoscience administrative team, I would like to say a big thank you for always being available. Thank you for the rapid responses and concerns even outside of academia. Your support throughout is highly appreciated.

**Andrea Hendricks and Luanne Thomas:** My close friends since first year, thank you for always being a phone call away, thank you for the encouragement and words of strength, you have no idea how it has helped me get through. I want to wish you guys all the best for your research and may you be successful in everything you do.



## FINANCIAL ASSISTANCE

---

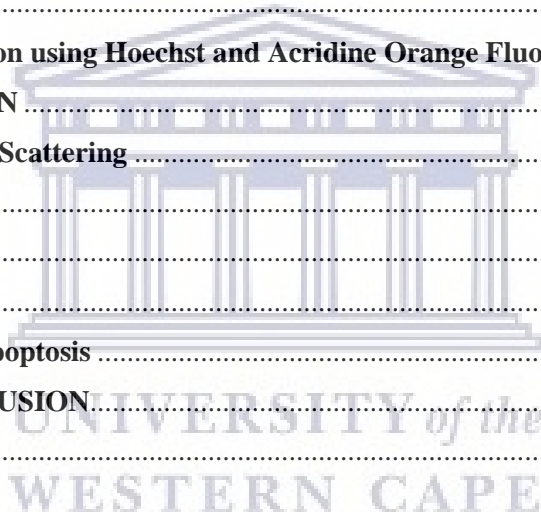
The financial support for this research project was provided by the Department of Science and Innovation in conjunction with the Department of Nanoscience at the University of the Western Cape. The opinions, predictions and conclusions made in this study are those of the writer and is not the views, opinions and conclusions of the funder. I would like to extend my sincere thankfulness for the support and investment.



# CONTENTS

DECLARATION.....	ii
ACKNOWLEDGMENTS .....	iii
FINANCIAL ASSISTANCE.....	v
CONTENTS.....	vi
ABBREVIATIONS .....	viii
LIST OF FIGURES .....	xi
LIST OF TABLES .....	xiii
ABSTRACT.....	xiv
<b>CHAPTER 1: INTRODUCTION.....</b>	<b>1</b>
<b>1.1. Cancer: a global burden.....</b>	<b>1</b>
1.1.1. Current treatment .....	1
<b>1.2. Nanotechnology .....</b>	<b>2</b>
<b>1.3. Gold nanoparticles (AuNP).....</b>	<b>2</b>
1.3.1. Synthesis of AuNP.....	2
1.3.2. Historic developments.....	3
1.3.3. Recent developments and Applications .....	4
<b>1.4. AuNP and cytotoxicity .....</b>	<b>5</b>
<b>1.5. Determinants of gold nanoparticle (AuNP) toxicity .....</b>	<b>6</b>
1.5.1. Size.....	6
1.5.2. Cell type.....	6
1.5.3. Surface charge and aggregation.....	7
<b>1.6. Genotoxicity.....</b>	<b>7</b>
<b>1.7. Gold Nanoparticles as radiosensitizing agents .....</b>	<b>8</b>
<b>1.8. Cellular uptake and localization of gold nanoparticles .....</b>	<b>8</b>
<b>1.9. AuNP in clinical settings.....</b>	<b>9</b>
<b>EXPERIMENTAL AIMS AND OBJECTIVES.....</b>	<b>11</b>
<b>CHAPTER 2: MATERIALS AND METHODS .....</b>	<b>12</b>
<b>2.1. Gold Nanoparticles (AuNPs).....</b>	<b>12</b>
2.1.1. AuNP Characterization .....	12
<b>2.2. AuNP treatment .....</b>	<b>13</b>
<b>2.3. Tissue Culture .....</b>	<b>15</b>
2.3.1. Reagents.....	15
2.3.2. Cell lines .....	15
2.3.3. Cell Culture and Conditions.....	15

<b>2.4. Cellular Proliferation and Viability Assays</b> .....	16
2.4.1. Crystal Violet Assay .....	16
2.4.2. WST-1 Assay .....	17
<b>2.5. Reactive Oxygen Species (ROS) Production Assay</b> .....	18
<b>2.6. Cell death detection using Hoechst and Acridine Orange Fluorescent Staining</b> .....	19
<b>2.7. Statistical Analysis:</b> .....	20
<b>CHAPTER 3: RESULTS</b> .....	21
<b>3.1. Gold nanoparticle characterization</b> .....	21
3.1.1. Dynamic Light Scattering (DLS).....	21
3.1.2. Zeta Potential (ZP).....	22
<b>3.2. Cellular Proliferation and Viability</b> .....	23
3.2.1. Crystal Violet .....	23
3.2.2. Cellular Viability.....	27
<b>3.3. Oxidative Stress</b> .....	31
<b>3.4. Cell death detection using Hoechst and Acridine Orange Fluorescent Staining</b> .....	35
<b>CHAPTER 4: DISCUSSION</b> .....	39
<b>4.1.1. Dynamic Light Scattering</b> .....	40
<b>4.2. Cell Proliferation</b> .....	41
<b>4.3. Cell Viability</b> .....	44
<b>4.4. Oxidative Stress</b> .....	45
<b>4.5. AuNP-induced Apoptosis</b> .....	47
<b>SUMMARY AND CONCLUSION</b> .....	48
<b>REFERENCES</b> .....	51



## ABBREVIATIONS

---

%	Percentage
° C	Degrees Celsius
>	Greater than
<	Smaller than
µg/ml	Micrograms per millilitres

### A

AuNPs	Gold nanoparticles
A549	Human lung carcinoma cells
AO	Acridine orange

### B

BSA	Bovine serum albumin
B16F10	Murine melanoma cells

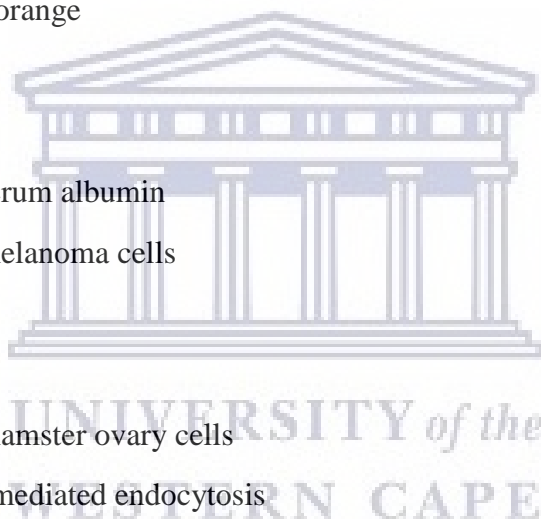
### C

CHOK1	Chinese hamster ovary cells
CME	Clathrin-mediated endocytosis
CV	Crystal violet

### D

dH <sub>2</sub> O	Distilled water
DMEM	Dulbecco's Modified Eagle Media
DMSO	Dimethyl sulfoxide
DCFH-DA	Dichloro-dihydro-fluorescein diacetate
DLS	Dynamic light scattering
DSB	Double stranded breaks

### E



EDL Electric double layer

## **F**

FBS Fetal bovine serum

## **G**

GSH Glutathione

GA Gum Arabic

## **H**

HepG2 Human hepatocellular carcinomas

HO Hoechst stain

HeLa Cervical cancer cells

## **I**

IV Intravenously

IP Intraperitoneal

## **K**

KVp Kilovoltage peak

## **M**

MRC5 Human lung fibroblasts

MVp Megavoltage peak

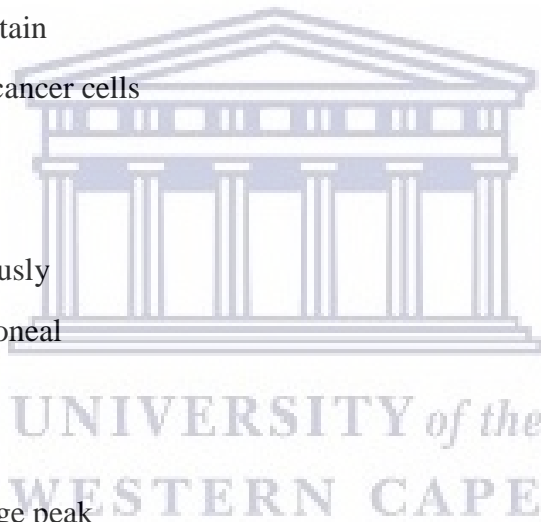
## **N**

NIR Near infrared

NIH3T3 Mouse embryonic fibroblasts

## **P**

PK-15 Porcine kidney cells



PBL Peripheral blood lymphocytes

PBS Phosphate buffered saline

PDI Polydispersity Index

## **R**

ROS Reactive oxygen species

RE Reticulo endothelial

R<sub>H</sub> Hydrodynamic radius

## **S**

SPR Surface plasmon resonance

## **T**

TOAB Tetrabutylammonium bromide

TC Tissue culture

## **U**

UV Ultra violet

## **Z**

ZP Zeta potential



## LIST OF FIGURES

CHAPTER 1.....	1
Figure 1.1: Global cancer incidence in 2018 across various continents.....	1
Figure 1. 2: (A) Image of colloidal gold samples after sodium citrate reduction. (B) with citrate ions ( $C_3H_5OCOO_3^{3-}$ ), and the different colours indicate different sized AuNPs with distinctive LSPR (C) UV–vis spectra for each gold (Au) solution .....	5
Figure 1.3: Biomedical applications of nanotherapeutics.....	5
CHAPTER 2.....	14
Figure 2. 1: DLS and Zeta potential analysis. ....	12
Figure 2. 2 : AuNP treatment.....	14
Figure 2.3: Experimental cell lines.....	16
Figure 2. 4 : Crystal Violet Assay.....	17
Figure 2.5: Hoechst 33324 and Acridine Orange Staining:.....	20
CHAPTER 3.....	22
Figure 3.1.1: Hydrodynamic size of AuNPs.....	21
Figure 3.2.1: The effects of AuNP size, concentration and exposure time on CHO-K1 cell viability.....	24
Figure 3.2.2: The effects of AuNP size, concentration and exposure time on A549 cell viability.....	26
Figure 3.2.3: Effects of AuNPs on CHOK1 cellular proliferations.....	28
Figure 3.2. 4: Effects of AuNPs on A549 cellular proliferations.. ..	29
Figure 3.3. 1: Detection of ROS production in CHOK1 cells.. ..	31
Figure 3.3.2: Detection of ROS production in A549 cells.....	33
Figure 3.4.1: Morphological changes of selected CHOK1 cells. Detected with a dual stain of Hoechst 33342 and acridine orange.....	36

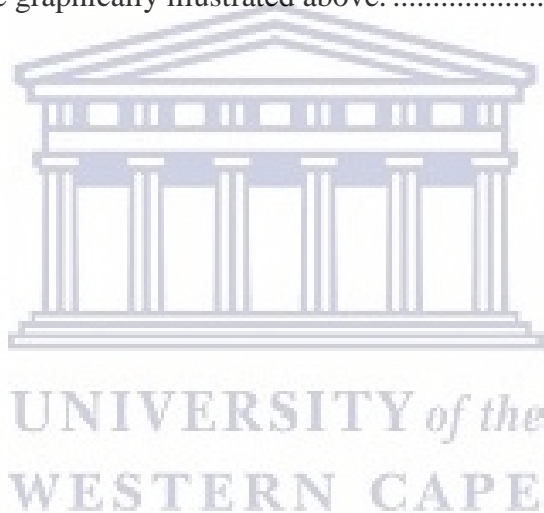
Figure 3.4.2: Morphological changes of selected A549 cells. Detected with a dual stain of Hoechst 33342 and acridine orange. ....37



## LIST OF TABLES

---

<b>CHAPTER 1</b> .....	1
Table 1 : Studies of AuNP biodistribution and toxicity in different <i>in vivo</i> models. ....	10
<b>CHAPTER 2</b> .....	14
Table 2: Volume extracted for treatment. Concentration values obtained was calculated per ml. The values represent the volume of AuNPs ( $\mu$ l) to be extracted to achieve the specific experimental concentrations for each size. ....	14
<b>CHAPTER 3</b> .....	22
Table 3: Zeta potential and DLS analysis of AuNPs. Analysis of DLS represents the hydrodynamic size dispersity curves (samples are averaged) and ZP depicts the charge and stability of NPs. Values are graphically illustrated above. ....	23



## ABSTRACT

---

Recently nanoparticles (NPs) have been introduced and used in combination with therapeutic approaches to develop nanotechnology-enabled medicine. These nanostructures allow for the exploitation of the physiochemical properties which may be beneficial in cancer treatment. The use of NPs in nanomedicine has proven successful in modern chemotherapeutics and has demonstrated promising potential in *in vivo* and *in vitro* radiosensitization studies. This is a baseline study aimed to determine the cytotoxic effects of AuNPs for potential radiosensitization analysis. The study analysed the effects of different AuNP sizes (30, 50 and 80nm), concentrations (5, 10 and 15  $\mu\text{g/ml}$ ) over various time periods in CHO-K1 and A549 cells. AuNPs were characterised by DLS and ZP analysis and showed that particles were moderately polydispersed and moderately to highly stable in charge. The effects on viability and metabolic activity of cells were determined using crystal violet and the WST-1 assay. Results from these assays showed that CHO-K1 cells are not tolerant to 48h exposure time and that 30 nm AuNPs had the most prominent cytotoxic effect. Proliferation for CHO-K1 cells was stimulated by 50 nm AuNPs across all concentrations after 4h treatment. A549 cells proved to be more tolerant to the treatments, after 48h compared to CHO-K1 cells. 50 nm and 80 nm AuNPs at 15  $\mu\text{g/ml}$  showed the greatest cytotoxic effect on A549 cells. Oxidative stress was observed in both CHO-K1 and A549 cells. After 24h ROS levels were significantly increased for all AuNP sizes and concentrations for both cell lines. Results for ROS correlated to that of crystal violet were at 15  $\mu\text{g/ml}$  or 50 nm and 80 nm significant oxidative stress was observed in A549 cells. Apoptosis was not extensive and thus was concluded that there was no AuNP-induced cell death in either cell line. CHO-K1 clearly showed a higher sensitivity to longer treatments and smaller AuNP particles (30 nm) in comparison to A549. CHO-K1 was stimulated by 50 nm AuNPs whilst the opposite was seen for A549 cells, thus the study concluded that AuNP treatment is highly cell-type and size-dependent. It can thus be postulated that 50 nm AuNPs could be an optimal probe for radiosensitization analysis, as it stimulated non-cancerous cells (CHO-K1) whilst having an anti-cancer effect on cancerous cells (A549). However, further investigation and research on a broader range of cell lines and parameters are required to have conclusive data for a particular cell model. This research may be utilized to determine AuNPs as radiosensitizing agents using various radiation modalities.

**Key Words:** *Gold nanoparticles, radiosensitization, cytotoxicity, Nanotechnology*

### 1.1.Cancer: a global burden

Cancer is a worldwide problem that has been estimated to have risen to 18.1 million newly diagnosed cases and 9.6 million deaths in the year 2018 (1). One in 5 men and one in 6 women globally, develop cancer in their lifetime and one in 8 men and one in 11 women will succumb to the disease. This increase in cancer incidences is attributed to numerous factors such as population growth, ageing and several environmental factors. The rise is particularly prevalent in rapidly developing economies, where a shift is detected from cancers related to poverty and infections to cancer linked to lifestyle and industrialization (1).

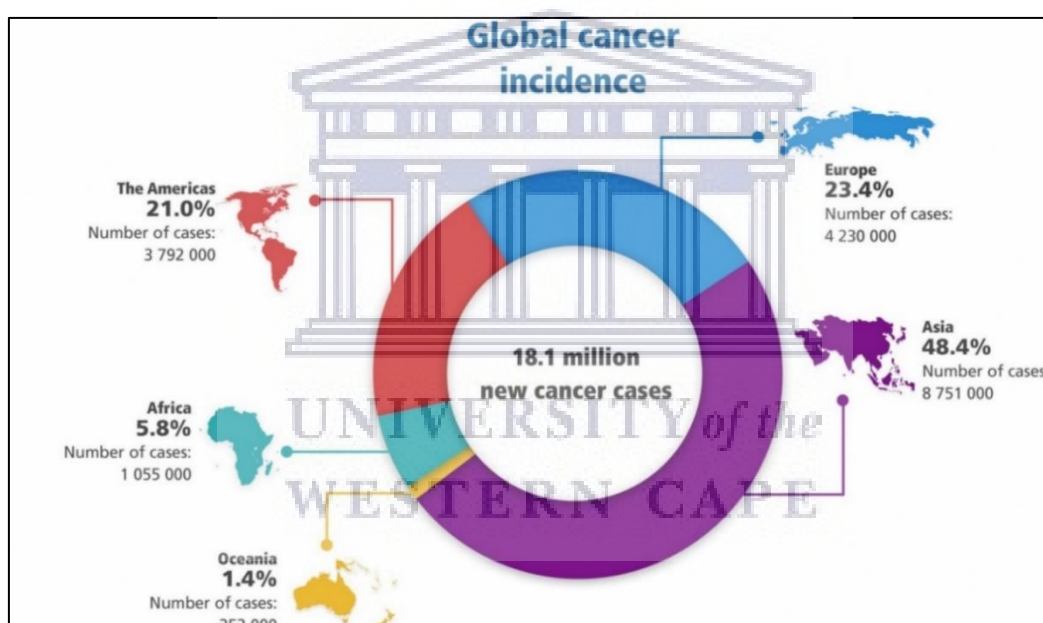


**Figure 1.1:** Global cancer incidence in 2018 across various continents. Image obtained from <https://www.uicc.org/news/new-global-cancer-data-globocan-2018>

#### 1.1.1. Current treatment

Lung and breast cancer are the leading types of cancers worldwide at approximately 21 million cases (1). Lung cancer is responsible for the most deaths (1.8 million, 18.4% in total) and it is most frequently diagnosed in men (14.5% in total). The current treatment options for cancer include chemotherapy, radiotherapy and surgery either delivered separately or in combination (2). These treatments come with some adverse effects and limitations. Surgery is confined to large, non-metastasized, accessible solid tumors and chemotherapeutic drugs exerts a cytotoxic

effect on rapidly proliferating cells. It is therefore ideal for malignant cells but has adverse effects due to the non-selective uptake by both cancerous and healthy cells (2).

Radiotherapy is an important treatment regime and about 50 % of cancer patients' receive radiotherapy using either Cobalt-<sup>60</sup> (<sup>60</sup>Co) gamma ( $\gamma$ ) rays, X-rays or neutrons (3). The main goal of radiation therapy is to deliver a sufficiently high dose to kill the tumour cells without damaging the surrounding healthy tissue and organs. Thus improving cancer treatments by focusing on tumour-targeted therapy and sparing healthy tissue, is vital (4). Advancements in the field includes contrast agents and radiosensitizer, such as iodine, gadolinium or gold, which are loaded into the tumour to improve the therapeutic ratio via increasing photon energy interactions in the immediate vicinity of the tumour, thus delivering a highly localized dose of radiation (5). Further advancements aim for organ-sparing methods which include; the usage of megavolt (MV) X-rays (6 – 25 MV) to avoid skin damage, better dosage concentration control via tomotherapy and intensity-modulated radiation therapy (IMRT) for the three-dimensional treatment of tumors.

## 1.2. Nanotechnology

Nanotechnology refers to a field of applied science where the goal is the control of matter at a scale of 1-100 nm (6). It is a multidisciplinary field that include pharmaceuticals, applied physics, material science, chemistry and electrical engineering (7). Nanoparticles (NPs) are minute naturally formed or manufactured sources of material, with properties that differ from that of the same respective bulk form. Generally, NPs possess distinct physiochemical properties including the small size, surface, electrical and optical properties (4,8). These particles display high surface absorptive capacity, bioavailability and enhanced cellular interaction (9).

## 1.3. Gold nanoparticles (AuNP)

### 1.3.1. Synthesis of AuNP

Gold nanoparticles (AuNPs) can be formed by various methods and synthesized via either physical or chemical approaches. Several subtypes of AuNPs exist, ranging in size, shape and physical properties. Of these the most well-known is the spherical AuNP. Both *in vitro* and *in vivo* studies are currently underway for AuNPs. Whilst *in vitro* studies are concerned with overall toxicity (i.e. to specific cell types) and modes of internalisation, *in vivo* studies investigate toxicity to disease causing elements (i.e. tumours), routes of administration, biodistribution, dosages, clearance of nanoparticles, and how AuNPs can be translated to the

clinical setting (10). Chemical synthesis is the most common synthesis method for metallic particles, however it is costly and the extensive use of toxic agents affect particle stability and biomedical application (11). The most common chemical, bottom-up methods are the Turkevich and Brust techniques. The Turkevich method was modified in 1973 by Frens (12) to obtain AuNPs with diameters of 15 to 50 nm. The main principle for the Turkevich method is based on the reduction of metal salts to form sphere-shaped, monodispersed AuNPs with dimensions of approximately 10-20 nm (13,14). Sodium salts of citrate are usually used as a reducing agent or stabilizer for the NPs, which prevents aggregation in colloidal suspensions. Additionally, UV-light, amino acids and ascorbic acid can be utilized in the place of citrate. This method was further modified by numerous researchers (15–18). Another stabilizer is Gum Arabic (GA). GA is a highly branched, non-toxic, slightly acidic polysaccharide that naturally exudates from acacia trees. GA contains glycoproteins and arabinogalactan-proteins (AGP) that are present in low and high molecular fractions, respectively. The presence of hydroxyl, carboxyl and amino acid allows that GA are sensitive to ionic strength and pH, these features make it an excellent stabilizer for nanoparticles (19,20).

In 1994 the Schiffrin-Brust method was first reported (11,14), it allowed for a simple approach to produce thermally stable and air stable AuNPs with controlled and low dispersity. This method was favourable for synthesizing AuNPs in organic solution with high stability. It is a two-phase process that utilizes tetrabutylammonium bromide (TOAB) as a phase-transfer agent from an organic to an inorganic solution, with this technique the particle sizes range from 2-6 nm in diameter.

### 1.3.2. Historic developments

Naturally occurring nanoparticles are the organic (polysaccharides and viruses) and inorganic (iron oxyhydroxides) compounds formed by events such as volcano eruptions and wildfires thus nanomaterials have existed in nature for many years (21). AuNPs were used to stain glass red during Roman times (14,22). Gold has long featured in medical history as a treatment for ailments ranging from nervous conditions and epilepsy in the 16th century, syphilis and tuberculosis in the 1920's, and in 1925 gold thiolates were used for the treatment of rheumatic diseases including psoriasis, juvenile arthritis, planindromic rheumatism and discoid lupus erythematosus (23). The use of AuNPs in immunochemistry and biological studies only began in 1971 when British researchers Falk and Taylor (24) used colloidal gold in antibody

conjugation, for direct electron microscopy, and visualization of surface antigens of salmonellae.

### 1.3.3. Recent developments and Applications

The frequent use of AuNPs in biomedical applications may be attributed to simple synthesis and versatile surface functionality to form new drugs that target cancer cells (8). Furthermore, these particles can be controlled by engineering processes to optimize shape, size and surface modifications to mention a few. It is these properties which make AuNPs an attractive nanomaterial in biomedicine, drug delivery systems (25), diagnostic imaging (26) and targeted therapy (27,28). The oscillating electromagnetic field of light makes a collective coherent oscillation of the free electrons of a metal and is also referred to as the conduction band electrons. The amplitude of the oscillation that reaches a maximum at a particular frequency is known as the surface plasmon resonance (SPR). Strong absorption of the incident light is caused by the SPR and can be measured with an ultraviolet (UV) - visible absorption spectrometer (see Figure 1.2). The SPR of noble gases such as gold are known to be stronger than that of other metals. Therefore the SPR wavelength of AuNPs can be altered from both visible and near-infrared (NIR) by manipulating the size, shape and structure of the particles. AuNPs can increase the scattering of light almost 6-fold greater than most absorbing organic dyes and fluoresceins. The scattering properties are size-, and shape-dependent (25) and makes AuNPs ideal for imaging and detection applications especially in cancer.

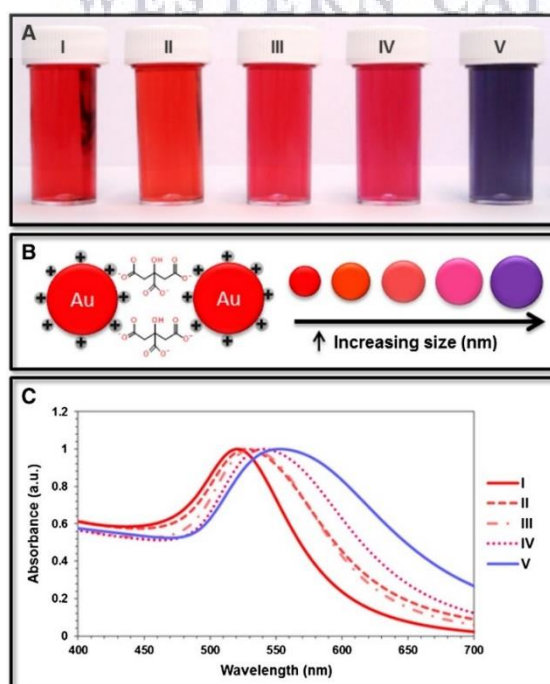


**Figure 1. 2:** (A) Image of colloidal gold samples after sodium citrate reduction. (B) with citrate ions ( $C_3H_5OCOO_3^{3-}$ ), and the different colours indicate different sized AuNPs with distinctive LSPR (C) UV-vis spectra for each gold (Au) solution (29)

AuNPs are used to deliver molecules into cells. Compared to the traditional chemotherapeutic drugs, the delivery via nanoparticles offer high concentration delivery of poorly water soluble drugs, protects drugs from the internal environments (stomach pH or lysosomes), target specific drug delivery to maximize treatment, controlled release of drugs and even combination therapy by the delivery of multiple drugs (30,31).

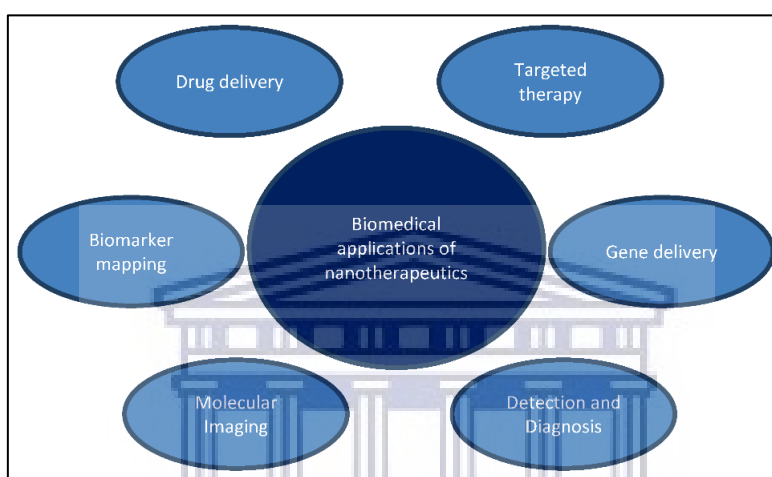


**Figure 1.3:** Biomedical applications of nanotherapeutics (32).

#### 1.4. AuNP and cytotoxicity

Nanoparticles are similar in size to typical cellular components and proteins and thus can pass natural mechanical barriers possibly causing adverse tissue reaction (33). With nanotechnology becoming a rapidly growing field nanoparticles are constantly studied for cytotoxicity, immunotoxicity and genotoxicity (34). Gold is considered an inert and nontoxic metal, however, when gold is altered to form AuNPs it exhibits higher reactivity due to the increased surface to volume ratio. As the ratio of surface area volume increases, the behaviour of surface atoms assume dominance over the interior thus leading to even small shape deviations modifying the interactions of the nanoparticle with its environment (38). Thus, due to the multitude of adjustable properties of AuNPs, seemingly contradictory reports of AuNP toxicity are available for both non-malignant and malignant *in vitro* and *in vivo* disease treatment (4,35). It has been reported that smaller NPs have the ability to penetrate deeper into tissue compared

to larger particles which tend to accumulate within cells and even various organs (36). A study by Connor *et al* (2005) investigated several AuNP (4, 12 and 18 nm) with different capping agents to determine the cytotoxicity effect. The study showed that sphere-shaped AuNPs entered the cells and did not induce cytotoxicity (37). Literature however, has reported that AuNP toxicity is associated with the dose side chain and stabilizer utilized (38,39), type of toxicity assay, cell line, as well as physical and chemical properties (40).

### **1.5.Determinants of gold nanoparticle (AuNP) toxicity**

#### 1.5.1. Size

In literature it has been discovered that a decrease in NP size is correlated to an increasing potential to penetrate cells and tissue, which enhances internalization and widespread distribution, but also an increased toxicity profile (4). A given dose of NPs from a particular source material can evoke a lethal effect in one size whereas for the same dose of that material at a different size no effect is induced. As mentioned above the AuNP size ( $D_{core}$ ) is a crucial parameter for determining cytotoxicity, AuNPs with a  $D_{core} < 2.0$  nm (smaller than 2.0 nm) are significantly toxic due to the ability to access the nucleus of a cell. When AuNPs have a  $D_{core} > 10$  nm cytotoxicity is weaker. In contrast to this statement, Vetten *et al* determined that 20 nm gold particles had a greater toxic effect on Chinese hamster ovary (CHO) cells than 14 nm particles indicating that cell types may be a parameter for cytotoxic testing (41).

Most reports on AuNP effects on cellular function focused on short-term exposure effects (2-12h), and not much on the long term (24h and longer). A study by Mironava *et al* (2010) examined 13 nm and 45 nm particles at various concentrations over 2-6 days and showed that after the sixth day both AuNP sizes accumulated in vacuoles and neither penetrated the nucleus or mitochondria. 45 nm gold particles at lower concentrations resulted in a significant increase in doubling time and thus an increase in cellular proliferation compared to 13 nm particles. The 13 nm gold particles proved to be most toxic as shown by the higher number of vacuoles since size and number of vacuoles relates to toxicity. The results showed that nanoparticle uptake proved to be size, concentration and time-dependent in human dermal fibroblasts (42).

#### 1.5.2. Cell type

Sik Suh *et al* (2013) reported that AuNPs (20 nM) enhanced cell differentiation and protected osteoblast cells against mitochondrial dysfunction (43). Chueh *et al* (2014) tested a variety of cytotoxic assays on several mammalian cell lines including PK-15 (porcine kidney), NIH3T3 (mouse embryonic fibroblasts), MRC5 (human normal lung fibroblasts) and Vero (African green monkey kidney). This study found that the  $IC_{50}$  (inhibition concentration of 50% of the

population) value differed among cells and that all cell lines displayed different sensitivity to the cytotoxic effects of AuNPs. The results proved that AuNPs should be assayed at different levels of organization in the organism to thoroughly determine the toxicity profile of that organism (35).

### 1.5.3. Surface charge and aggregation

AuNP aggregation in cells results in increased reactive oxygen species (ROS) production and so affecting cellular function (4). Smaller particles tend to aggregate less whilst the larger particles inside cells are more susceptible to aggregation and cytotoxicity (44). Another cytotoxic determinant is NP surface charge, AuNPs with different surface charges have also been reported to demonstrate varying toxicity: small, positively charged particles pass through cell membranes and cause cytotoxic effects (45) yet anionic AuNPs demonstrate no toxic effects. Furthermore, negatively charged particles bind less efficiently to the similarly charged cell membrane due to electrostatic repulsion forces inhibiting the nanoparticles from entry. To internalise negatively charged molecules into the cell, cationic ions are necessary to interact with the negatively charged cell membrane and particle surface to mediate charge-mediated endocytosis (46).

## 1.6. Genotoxicity

Genotoxicity is an important experimental parameter when analysing different agents or stressors such as NPs. The inconsistency of AuNP induced genotoxicity in literature is attributed to the variation in NP shape, size, coating, concentration, exposure time and experimental conditions. There are numerous *in vitro* and *in vivo* mechanisms to examine the genotoxic potential of a given nanomaterial. A study conducted by Xia *et al* (2017) investigated human hepatocyte (HepG2) to assess AuNP induced DNA damage via the comet assay. The results showed that DNA damage occurred through strand breaks. The strand breaks were highly size-dependent as 5 nm gold particles induced DNA damage whereas particles between 20-50 nm did not result in any significant damage (47). Nanoparticle size has shown to be an important determinant in the genotoxicity profile however Ishidate *et al* (1998) found that exposure time also plays a vital role (48). A possible underlying mechanism may be that the longer the exposure time the greater the AuNP accumulation in cells or tissue which increases the likelihood of DNA damage. Although the precise underlying phenomenon for genotoxicity is not known there are several proposed theories to explain the effect of metallic NPs. The first refers to the direct interaction between genetic material and metal NPs. This interaction may

result in physical and chemical damage to the DNA. The second refers to indirect DNA damage and this is due to the production of reactive oxygen species (ROS). The production of ROS affects biomolecules, proteins lipids and genetic material (47).

### **1.7. Gold Nanoparticles as radiosensitizing agents**

Over the last few years there has been a considerable interest in the use of formulations to enhance radiotherapeutics effects, especially using metal (mainly gold) based nanoparticles. AuNPs as radiosensitizer can improve the therapeutic gain by delivering a highly localised dose of radiation to the vicinity of a tumour (49). High atomic mass contrast agents, such as gold (atomic mass = 79) provide the greatest probability for photon interactions by photoelectric effect (50). Furthermore, the photoelectric effect generates a high linear energy transfer wherein the short range of the photoelectric interactions produce photoelectrons and Auger electrons which introduce a localised dose enhancement in the tumour (50). Auger electrons are weakly bound electrons ejected from an atom as a result of electronic shell rearrangements, and are very effective in producing extremely high local ionisation density damage such as alpha ( $\alpha$ ) particles (49). Studies have found that 50 nm naked AuNPs possess strong radiosensitivity in comparison to smaller and larger AuNPs. Chithrani *et al* (2010) observed differences in the radiosensitizing effect between AuNP sizes of 14, 50 and 74 nm. The study showed that 50 nm AuNPs could act as radiosensitizer in both lower and higher photon energy ranges with dose modifications of 1.66 for kVp and 1.17 for MVp (51). An increase in lethal double-stranded DNA breaks (DSBs) was observed in the presence of AuNPs. The more DSB observed, the less chance of DNA repair and the greater the chance of cell death (51).

Besides AuNPs serving as photon-absorbing agents, it also intensifies radiation damage by causing cell cycle acceleration (52), cytokinesis arrest, increases programmed cell death (53,54) thus proving to be a biologically active agent. Overall gold (thus AuNP) with its high atomic number would cause increased electron emission resulting in the increased production of free radicals and greater DNA damage causing cell death (55).

### **1.8. Cellular uptake and localization of gold nanoparticles**

As mentioned above, bio-distribution and cellular uptake of AuNPs are size-dependent (56,57) and surface properties play a major role in the uptake process (58). Various mechanisms for

nanoparticle internalisation have been suggested, including phagocytosis, micro-pinocytosis, and receptor-mediated endocytosis pathways including caveolae-mediated, clathrin-mediated, and caveolae/clathrin-independent endocytosis via receptors and cell-signalling cascades (59–61).

Pinocytosis and non-specific endocytosis has been reported to occur for particles smaller than 100 nm and phagocytosis for larger than 100 nm (58). The optimal size for cellular uptake and retention of AuNPs was found to be 50 nm (62). AuNPs smaller than 30 nm has the ability to enter and leave the cell via passive diffusion (63). Small, positively charged NPs can pass through the cell membrane leading to membrane rupturing and adverse cytotoxic effects (45,64).

### **1.9. AuNP in clinical settings**

There has been positive progress in nanotechnology-based cancer diagnosis, and a few studies have already progressed to clinical trials (65). Requirements include modified particle design that prevents clearance and uptake by the reticuloendothelial (RE) system. Secondly, the nanoparticles must be able to alter the biodistribution of the drug load to allow uptake at the diseased site whilst preventing uptake by healthy tissue (66).

Studies show that most intravenously (IV) administered NPs are distributed into healthy tissue mainly in phagocytic cell-rich organs like the liver and spleen before being cleared by the renal system. As mentioned before, although the gold core is known to be inert and non-toxic, significant toxicity can be caused by AuNP synthesis methods, the physiochemical properties of AuNPs, surface conjugates, dosage and the route of administration. Thus, numerous studies have been undertaken to analyse and determine the *in vivo* behaviour such as biodistribution, accumulation in tissue and renal clearance (67–69). A report by Zhang *et al* (2012) investigated AuNP biodistribution and toxicity of glutathione (GSH) and bovine serum albumin (BSA) using mice as an *in vivo* model. The results showed that smaller 2nm GSH-coated AuNPs caused efficient kidney removal and were readily metabolized compared to larger 8 nm BSA-coated particles. Both particles caused acute infection, inflammation and damage to kidney function after 24h exposure. The 2 nm diameter AuNP effects were gone after 28 days while the 8 nm particles continued accumulating in the liver and spleen resulting in irreversible toxicity (70).

There are numerous *in vivo* studies shown in **Table 1** investigating biodistribution, toxicity and accumulation of AuNPs in animal models. These studies ultimately strive to observe both the beneficial and adverse effects of various parameters on an organism system as a whole, with an end goal to apply the knowledge and data to the bettering of treatment and diagnosis. The understanding of how AuNPs behave *in vitro* is thus the stepping stone to altering methodology and technique for *in vivo* application.

**Table 1 : Studies of AuNP biodistribution and toxicity in different *in vivo* models.**

AuNPs size (nm)	Dosage	Route of administration	Animal model	Exposure time	References
21	7.85 $\mu\text{g}$ AuNPs/g	IP	Male C57BL/6 mice	1, 24, 72 h	(68)
4, 100	4.26 $\text{mg}\cdot\text{kg}^{-1}$	IV	Male BALB/C mice	30 min	(71)
3, 5, 8, 12, 17, 37, 50, 100	8 $\text{mg}\cdot\text{kg}^{-1}$	IP	Mice		(69)
13	0.04, 0.2, 0.4 $\text{mg}\cdot\text{kg}^{-1}$	IP	C57BL/6 mice	8 days	(72)
20, 100	1 $\text{g}\cdot\text{kg}^{-1}$	IV	C57BL/6 mice	24 h	(73)
40	0.5 ml	IV	Female C57BL/6 mice	1 day 1, 3, 6 month	(74)
20	0.01, 0.015 mg Au/kg	IV	Rats	1, 7 days 1,2 months	(75)
13	0.17, 0.85, 4.26 $\text{mg}\cdot\text{kg}^{-1}$	IV	Male BALB/C mice	5, 30 min 4, 24 h 7 days	(76)
10, 30, 60	0.4 ml	IP	Male Wistar rats	16 , 32 h	(77)

***Intravenous (IV), intraperitoneal (IP)***

## EXPERIMENTAL AIMS AND OBJECTIVES

---

AuNPs are known for its unique properties that aid in biomedical applications however, there still exist many contradictions on the effects of AuNPs in different cells or systems.

This study investigates the effects of various AuNP sizes (30nm, 50nm and 80nm) and concentrations (5, 10 and 15  $\mu\text{g/ml}$ ) over different exposure times (4h, 24h and 48h) in a normal- and malignant cell line. The study presents as baseline research with the intent of determining the optimal size, dose and time of exposure of AuNPs to be deployed as radiosensitizing agents in both cancerous and non-cancerous cells. The results will pave the way for future studies in which the radiosensitization effects of AuNPs in both cancerous and non-cancerous cells will be investigated by using different radiation types available at iThemba LABS (South Africa, Cape town).

### **The study aims to:**

1. To obtain the optimal size, concentration and time-dependent effects of AuNPs on CHO-K1 (non-cancerous) and A549 (cancerous) cells for future radiosensitization studies
2. Investigate the effects of AuNP treatment on cell viability and proliferation.
3. Determine the level of ROS production by CHOK1 and A549 using the H2DCF-DA fluorescent assay.
4. Study AuNP-induced changes in nuclear and cellular morphology via Hoechst and acridine orange staining.

## CHAPTER 2: MATERIALS AND METHODS

---

### 2.1. Gold Nanoparticles (AuNPs)

Commercially available citrate stabilized, colloidal gold nanoparticles sized 30, 50 and 80 nm were purchased from Sigma Aldrich (South Africa). Each size was purchased in 100 ml quantities and stored according to the manufacturer's instructions. All AuNPs were filtered through 0.2  $\mu\text{m}$  filters (Whatman, Lasec) and aliquoted prior to use to ensure sterility.

#### 2.1.1. AuNP Characterization

##### 2.1.1.1. Size and Zeta Potential (ZP)

Characterization of AuNPs is important as physical and chemical properties of NPs play a vital role in the behaviour within a biological system (78). Size and surface charge of NPs are the two most common physiochemical properties known for their contribution to biological effects such as particle uptake and toxicity (42). The dynamic light scattering (DLS) utilizes colloidal dispersion properties to deduce the hydrodynamic radius ( $R_H$ ) (79) and is the preferred technique to use as the hydrodynamic size of a particle in solution is usually larger than the actual particle size when observed microscopy (80). The zeta potential (ZP) reflects the difference in potential between the electric double layers (EDL) of electrophoretically moveable particles and the layer of dispersant present around the slipping plane.

In this particular study, all gold nanoparticle samples underwent a 1:10 dilution, the characterization method was done by pipetting 1 ml of AuNP sample into a cuvette. The NPs were then analysed using a Zetasizer Nano ZS (Malvern). Samples were characterized at 25°C in a dispersant of distilled water ( $\text{dH}_2\text{O}$ ).

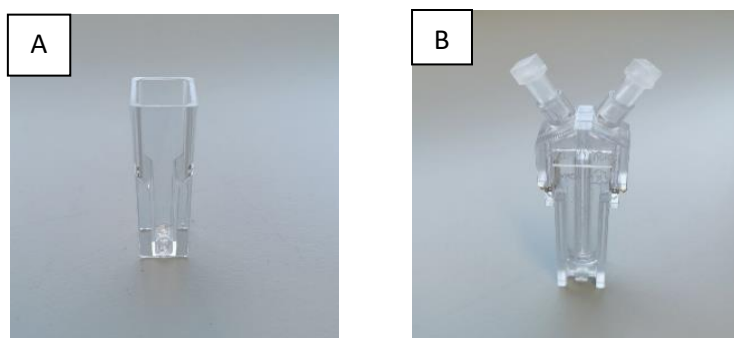


**Figure 2. 1: DLS and Zeta potential analysis.** [A] 1 ml clear cuvette for DLS analysis. [B] DTS1070 electrode cell/cuvette for zeta potential analysis.

## 2.2. AuNP treatment

A mathematical equation was applied to determine the volume of commercial AuNP solution needed to expose/treat cells, with a required experimental concentration. The calculated volume indicates the amount of AuNP solution needed per ml to achieve the required concentration. In this study, the used AuNP sizes were 30, 50 and 80 nm at concentrations of 5, 10 and 15 µg/ml. Firstly the radius of each particle was determined.

### *Radius*

$$r = \frac{d}{2}$$

Convert nm to cm by multiplying  $10^{-7}$

d= diameter (commercial AuNP size chosen for experiment).

### *Volume of one particle*

$$V = \frac{4}{3} \pi r^3$$

$\pi = 3.142$

Volume of one particle is in  $\text{cm}^3$

### *Mass of one particle*

$$M = V \cdot \rho$$

- Density of gold= $\rho=19.32$  g/ml
- Unit is in g

### *No. of particles needed*

$$\text{NumParticlesNeeded} = \frac{\text{experimental concentration}}{M}$$

- Chosen concentration is the experimental concentration (in this study 5, 10 and 15 µg/ml)
- Convert to grams

E.g.  $5 \times 10^{-6}$  (5µg/ml)

### *Particles per ml*

Particles per ml are indicated by the manufacturer (Sigma Aldrich)

E.g. 30 nm particles/ml value is  $1.8 \times 10^{11}$  particles/ml

**Volume for extracted amount**

$$Volume = \frac{NumParticlesNeeded}{Particles\ per\ ml}$$

Volume (amount) in ml extracted from the bottle to yield the desired experimental concentration.

Convert ml to  $\mu$ l

**Table 2: Volume extracted for treatment. Concentration values obtained was calculated per ml. The values represent the volume of AuNPs ( $\mu$ l) to be extracted to achieve the specific experimental concentrations for each size**

AuNP Size (nm)	Control	5 $\mu$ g/ml	10 $\mu$ g/ml	15 $\mu$ g/ml
30	0 $\mu$ l	101,6 $\mu$ l	203,8 $\mu$ l	306 $\mu$ l
50	0 $\mu$ l	114,9 $\mu$ l	228,9 $\mu$ l	342,9 $\mu$ l
80	0 $\mu$ l	123,9 $\mu$ l	247,9 $\mu$ l	371,9 $\mu$ l

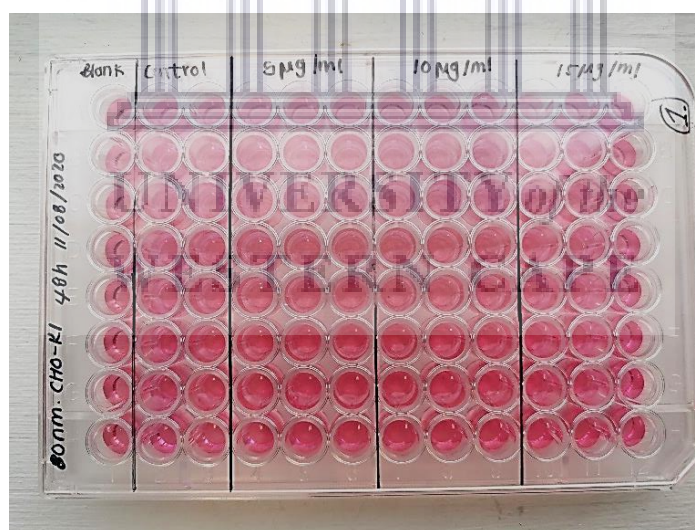


**Figure 2. 2 : AuNP treatment.** Typical 96 well plate set up for AuNP treatment exposure on CHOK1 cells.

Several 96 well, clear, flat bottom, TC treated culture plates' (Nest®) were prepared with a blank, control and various concentrations of AuNPs prepared using the calculation above. Volumes varied based on the different sizes and concentrations required. For each assay A549 and CHOK1 cells were treated accordingly.

## 2.3. Tissue Culture

### 2.3.1. Reagents

Sterile filtered fetal bovine serum (FBS) (WhiteSci), penicillin (5000 unit/mL) and streptomycin (5000 µg/mL) and 1X Trypsin-EDTA (Sigma Aldrich, South Africa). RPMI 1640 (1X, 2.05 mM L-glutamine), DMEM (4.5 g/l glucose, L-glutamine) (WhiteSci) and phosphate buffered saline (PBS) (Separations Scientific SA).

### 2.3.2. Cell lines

CHO-K1 (Chinese Hamster Ovarian) cells, an adherent epithelial-like cell was gifted by Dr. Charlot Vandevoorde (NRF-iThemba LABS, Somerset West, Cape Town). The experimental A549 cells, an adenocarcinoma human alveolar basal epithelial cell was gifted by Prof. Mervin Meyer (Biotechnology Department, University of the Western Cape). Both cell lines were originally purchased from ATCC, Maryland USA. CHOK1 was selected as the control cell line to indicate the effects of the experimental conditions on normal (non-cancerous) cells whilst A549 was selected to compare and contrast the effects on malignant cells

### 2.3.3. Cell Culture and Conditions

CHO-K1 (Chinese Hamster Ovarian) and A549 (Human lung carcinoma) cells were routinely maintained in RPMI 1640 (Lonza) and DMEM (Lonza), respectively. Media was supplemented with 5% filtered FBS and 0.4% penicillin (5000 unit/ml) and streptomycin (5000 µg/ml). Cells were grown in standard conditions of 95% humidity, 5% CO<sub>2</sub> at 37°C. Growth media was replenished every 2-3 days if necessary until cells were suitable to harvest and plating for experimentation. Cells were used at low passage number of 32 and 5 for CHOK1 and A549, respectively and multiple stocks were made and stored at -80°C.

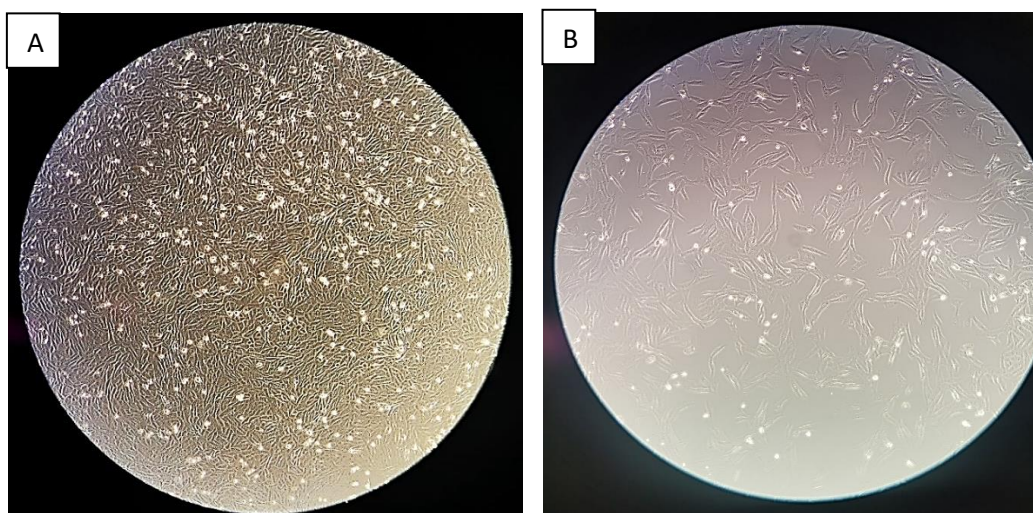


**Figure 2.3: Experimental cell lines.** [A] CHO-K1 cell line reached confluency and displays multiple dividing cells. [B] A549 cell line with a confluency of approximately 75-80% and displaying dividing cells. A549 and CHO-K1 cell lines were cultured in RPMI 1640 and DMEM. [C] Cell culture stock at low passage number stored at -80°C. All experiments were done in biological triplicates.

## 2.4. Cellular Proliferation and Viability Assays

Viability and/or proliferation of cells are good indicators of cellular growth and health. Various physical and chemical substances affect the health and metabolism of cells in different ways. These substances may cause cytotoxicity through numerous mechanisms including cell membrane destruction, altered protein synthesis, altered DNA processes and blocking of receptor sites. In vitro cell viability and toxicity tests are commonly performed on cultured cells. Recently toxicity assays have been employed in oncology research to analyse the toxicity profiles and tumour cell growth inhibition by different drugs (33, 34, 81). These assay mechanisms differ based on cell functions like membrane permeability, adhesion, ATP production, enzyme activity and uptake (82). Based on the doubling time of both A549 and CHO-K1 (20-22h) cells, the seeding density in 96 well clear, flat bottom plates were set at 1500, 2000 and 2500 cells/well for 48, 24 and 4h respectively, cells were then allowed to grow/attach overnight. Biological triplicates of each experiment was performed.

### 2.4.1. Crystal Violet Assay

Viable cells in culture attach to tissue culture plate surfaces, however during cell death cells lose their adherent properties and detach from culture plates. This mechanism is then exploited to assess cell death and determine rate of proliferation when stimulated with cytotoxic agents. Crystal violet (CV) dye binds to DNA and protein of viable cells resulting in staining. It is a colorimetric assay allowing the assessment of cell proliferation. Dying cells are lost from the attached cell population, thus when CV is applied the amount of staining is reduced in culture aiding in proliferation assessment (83, 84).

Cells (A549 and CHO-K1) were seeded at cell densities of 2500 cells/well into 96-well microplates (Nest ®). Cells were then incubated at 37°C overnight to allow for attachment. Cells were treated and exposed with various AuNP sizes, concentrations and time intervals based on the calculation (see *section 2.1.3*). The experiment was terminated by removing growth media and addition of 100 µl of 1% (v/v) glutaraldehyde (Sigma Aldrich, South Africa) following incubation. Samples were incubated for 15 minutes at room temperature (RT), the glutaraldehyde discarded. 100 µl of 0.1% (w/v) CV stain added. After a 30 minute incubation time at RT, plates were submerged in running water for 15 minutes to ensure removal of excess

stain. The plates were left to dry for up to 1 week. Prior to reading, 200  $\mu$ l of 0.2 % (v/v) Triton X (Sigma Aldrich) was added to the samples and incubated for 30 minutes at RT. 100  $\mu$ l of the liquid content was transferred to a 96-well microtiter reading plate using reverse pipetting. Sample absorbance was analysed using an EZ Read 400 microplate reader and read at a wavelength of 570 nm.

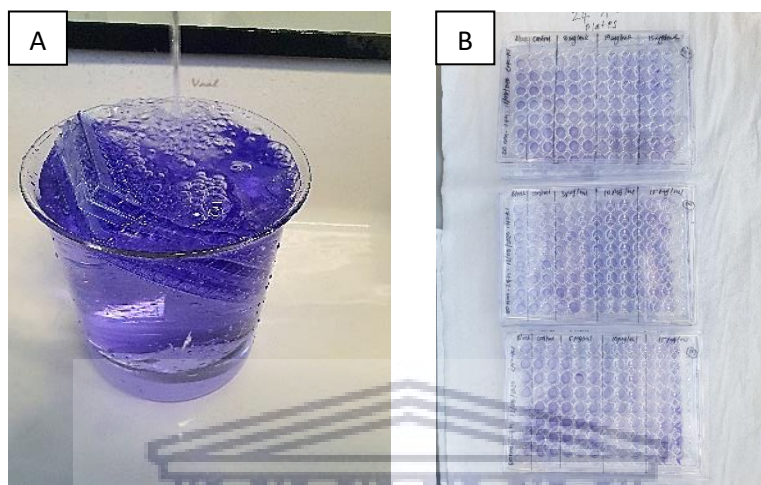


**Figure 2. 4 : Crystal Violet Assay.** [A] Samples submerged in water to ensure removal of excess dye. [B] Post staining, samples left to dry.

#### 2.4.2. WST-1 Assay

The WST-1 colorimetric assay was selected to determine cell viability thus confirming the relative proliferation rate obtained with the crystal violet assay of the CHOK1 and A549 cells treated with the different AuNPs. The principle of WST-1 (2-(4-iodophenyl)-3-(4-nitrophenyl)-5-(2, 4-disulfophenyl)-2H tetrazolium monosodium salt is the formation of a water-soluble formazan from WST-1 (tetrazolium salts) by mitochondrial dehydrogenase enzyme in the presence of intermediate electron acceptor. The chemical reaction results in a colour change that is proportional to the amount of mitochondrial dehydrogenase and thus proportional to the amount of metabolically active cells (82).

Both A549 and CHO-K1 (adherent cells) were seeded at 5000 cells/well with a final volume of 200  $\mu$ l, cells were then incubated overnight to obtain sub-confluency at 37  $^{\circ}$ C and 5% CO<sub>2</sub>. After 24h, cells were treated with suitable AuNP sizes and concentrations to a final volume of 50  $\mu$ l per well. Treated cells were then incubated for 4 and 24h. The experiment performed for each selected time period contained a solvent control, positive and negative (untreated cells)

controls. The positive control for this cytotoxicity assay was 50  $\mu$ l of 10% DMSO to induce toxicity. The metabolic activity of the controls and treated samples were then determined by the addition of the WST-1 reagent (Sigma Aldrich, South Africa). 5  $\mu$ L of WST-1 reagent was added to each well and incubated at standard conditions for 3h. WST-1 formazan was measured and read at a wavelength of 460 nm and a reference wavelength of 620 nm using an EZ Read 400 microplate reader and data was analysed via Galapagos Expert 1.0.0.0 software. The percentage of cell proliferation was obtained by:

$$\frac{\text{Absorbance}_{\text{treated cells}}}{\text{Absorbance}_{\text{control cells}}} \times 100$$

Data was expressed as mean  $\pm$  SD. The change in cellular proliferation between the control and treated samples were considered statistically significant with a p-value < 0.05, P<0.001 and P<0.0001.

### **2.5.Reactive Oxygen Species (ROS) Production Assay**

DCFH-DA is used for the detection of intercellular reactive oxygen species (ROS) production and oxidative stress. This probe is cell-permeable and is hydrolysed to the DCFH carboxylate anion which remains within the cell. In the presence of ROS, the two-electron oxidation of DCFH produces dichlorofluorescein (DCF), a fluorescent product that can be detected by various procedures such as flow cytometry, fluorescent microscopy and via a fluorescent plate reader (85). Several studies have shown that metal salts and ions such as AuNPs that possess reactive sites on their surfaces have the ability to elicit oxidative stress via the production of ROS (86–88).

Biological triplicates of CHO-K1 and A549 cells were seeded at 2500 cells/well in a 96-well clear, flat bottom plate and incubated overnight at 37°C and 5% CO<sub>2</sub> to allow for attachment. A 10 mM (w/v) stock solution of carboxy-H<sub>2</sub>DCFDA (Whitehead Scientific, South Africa) was prepared by dissolving 19.5 mg of H<sub>2</sub>DCFDA in 4 ml absolute ethanol. Prior to use, a final working concentration of 2  $\mu$ M was prepared in serum reduced media (2%). Culture media was then removed and cells washed with PBS to remove any trace of original media. Plates were covered with insulation tape and aluminium foil to ensure protection from light. Samples were loaded with 100  $\mu$ l of working carboxy-H<sub>2</sub>DCFDA dye solution and incubated in the dark for 30 minutes at 37°C. The carboxy-H<sub>2</sub>DCFDA dye was removed and cells were washed twice with PBS. Cells were then treated as mentioned in *section 2.1.3* and incubated

accordingly. Once exposure time was completed media was removed and cells were washed in PBS (100  $\mu$ l of PBS was added to each sample) and the production of ROS was analysed via the FluoStar Omega plate reader at excitation and emission wavelengths of 485 and 530 nm, respectively.

## **2.6. Cell death detection using Hoechst and Acridine Orange Fluorescent Staining**

Hoechst's is a bisbenzimidazole dye used to stain DNA. The dye is excited by UV lasers, mercury-arc lamps or UV light of xenon at approximately 360 nm. It produces a spectrum of blue light (460 nm). It is a non-intercalating dye that binds to the small groove at A-T-rich areas. Hoechst 33342 (HO) is a blue fluorescent dye that has the ability to stain chromatin DNA (98). When Hoechst's binds to DNA the fluorescence intensifies by 30 fold producing a decent signal-to-noise ratio. Acridine orange (AO) is a weak basic dye that is able to penetrate cells. AO possess metachromatic characteristics, when excited with blue light at approximately 488 nm in monomer form, it fluoresces green whilst in dimer for the fluorescence is orange. The main features of apoptosis such as chromatin condensation and fragmentation can be observed clearly with HO while autophagosomes in cells undergoing autophagy, is shown AO. AO acts as a pH indicator in living cells, accumulating within acidic compartments (autophagosomes containing lysosomes) and fluoresces orange/red. When observing morphological changes of nuclei, healthy nuclei are round and even stained and apoptotic nuclei are usually smaller or even fragmented and fluoresce more intensely due to the condensation of DNA. When cells are in mitosis, DNA may appear condensed as apoptotic cells however are distinguishable by finger-like protrusions indicating chromosome separation. Cells in necrosis are swollen, have no condensed DNA and cell edges are not clear or well-defined (89).

Exponentially growing A549 and CHO-K1 cells were seeded at a cell density of 5000 cells/per well in  $\mu$ -Slide 8-well chamber slides (Sigma Aldrich).  $\mu$ -Slides were incubated at 37 °C for 24 hours to allow cell attachment. Samples were then treated according to selected times, AuNP concentrations and sizes as in *section 2.1.3*. Hoechst (HO) 33324 (Sigma Aldrich, South Africa) stock solution (10 mg/ml) was made up and diluted in growth media to give a final working concentration of 1  $\mu$ g/ml. A stock solution of acridine orange (AO) was prepared by dissolving 50 mg AO in 10 ml dH<sub>2</sub>O (5mg/ml). A 1 $\mu$ g/ml working solution was then prepared. After the incubation period for each selected time was completed 100  $\mu$ l of HO solution was added to the chambers and incubated at 37 °C for 30 minutes, 25 minutes into the incubation 100  $\mu$ l of 1  $\mu$ g/ml AO was added to each chamber and left for the remaining 5 minutes. The HO/AO solution was then removed and cells were washed with PBS to remove excess stain.

$\mu$ -Slides were then left to dry for several minutes in a dark area and cell nuclei was then analysed with a fluorescent microscope (Zeiss) at excitation/emission of 350 and 461 nm. To prevent fluorescent quenching all samples were stored and examined in a dark room.

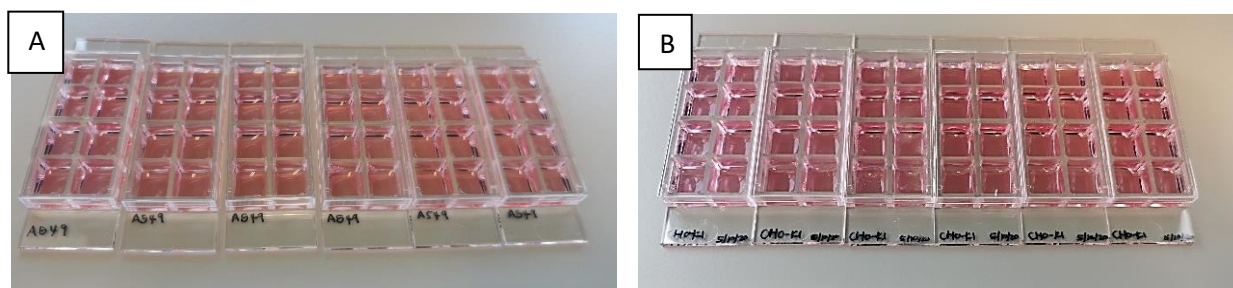


**Figure 2.5: Hoechst 33324 and Acridine Orange Staining:** [A] A549 samples and [B] CHO-K1 samples. Cells were treated with AuNPs at various concentrations and sizes in 8-well  $\mu$ -Slides chamber slides and stained with HO 33324 and acridine orange fluorescent stain to analyse morphological changes in cell nuclei.

### 2.7. Statistical Analysis:

Crystal violet, WST-1 and the ROS assays' statistical analysis were carried out using Microsoft Excel 2013 and GraphPad Prism® 5. All the experiments were done in biological triplicates. Microsoft Excel 2013 was utilized to correct data, calculate averages for and to establish a factor allowing results to be expressed as a percentage. Results were imported into GraphPad Prism® 5 for graphical representation and statistical analysis. Grouped Bar graphs were used to represent the data and error bars. Two-way analysis of variance (ANOVA), and Bonferroni post-test was used to obtain statistical significance between the different treatment options and control samples. The variation between groups were considered statistically significant when  $P < 0.05$ , highly significant when  $P < 0.01$ , and extremely significant when  $P < 0.001$ .

## CHAPTER 3: RESULTS

### 3.1. Gold nanoparticle characterization

#### 3.1.1. Dynamic Light Scattering (DLS)

DLS also known as photo correlation spectroscopy is a technique used to determine hydrodynamic size (90). The polydispersity index (PDI) for DLS represents the intensity of scattered light by different fractions of particles with varying sizes.  $PDI \leq 0.1$  is considered as monodispersed. Values between 0.1-0.4 are moderately polydispersed and  $>0.4$  are considered highly polydispersed (78).

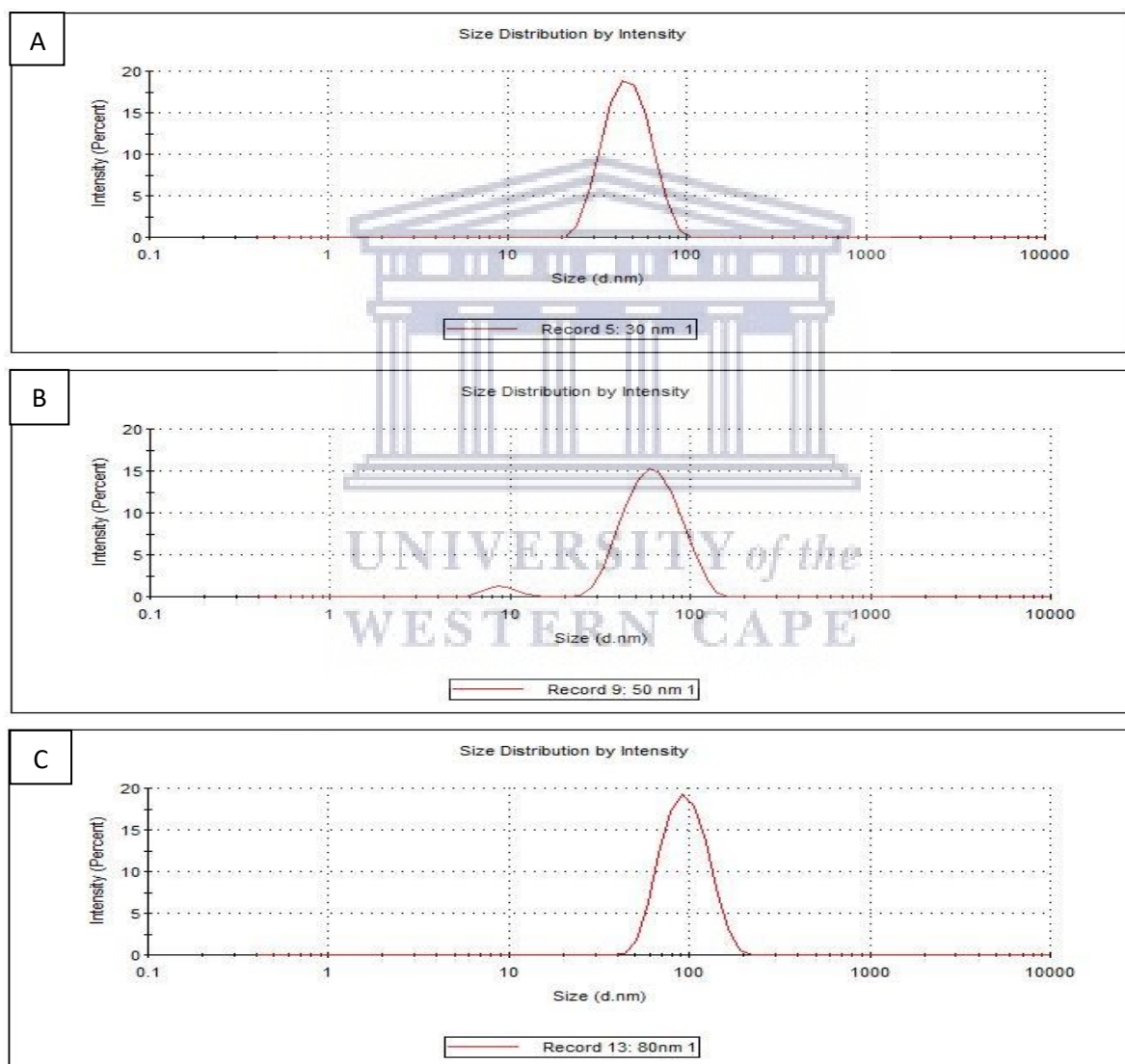


**Figure 3.1.1: Hydrodynamic size of AuNPs.** [A] 30 nm AuNPs (d.nm), [B] 50nm AuNPs (d.nm) and [C] 80 nm AuNPs (d.nm) at 25°C in in a dispersant of distilled water (dH<sub>2</sub>O).

All samples are moderately polydispersed and produced good quality reports based on Bhattacharjee (2016). It is rare that NP mixtures are 100% monodispersed and guidelines stipulate that more than 50% of the NPs within the mixture must be  $\leq 100$  nm to categorise it as a nanoparticle mixture (78). The mean Z-average diameter for 30 nm particles is 41.16 d.nm and 80 nm is 86.75 d.nm this is due to the DLS technique measuring  $R_H$  and thus producing a value larger than the depicted NP size. 50 nm particles produced a smaller value at 48.24 d.nm. The PDI for all samples are stable, moderately polydispersed. PDI was found at 0.124 for 30nm, 0.282 for 50nm and 0.196 for 80nm

### 3.1.2. Zeta Potential (ZP)

ZP referred to as electrokinetic potential is the potential at the slipping plane of a colloid particle under an electric field (91).

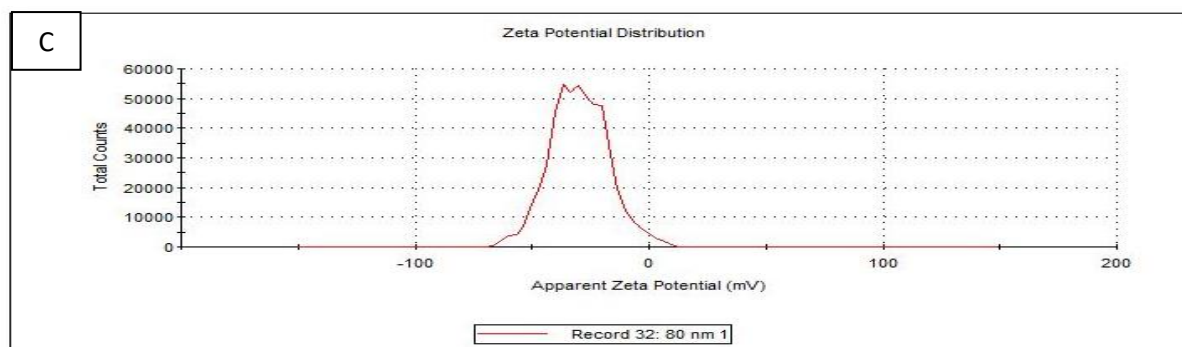
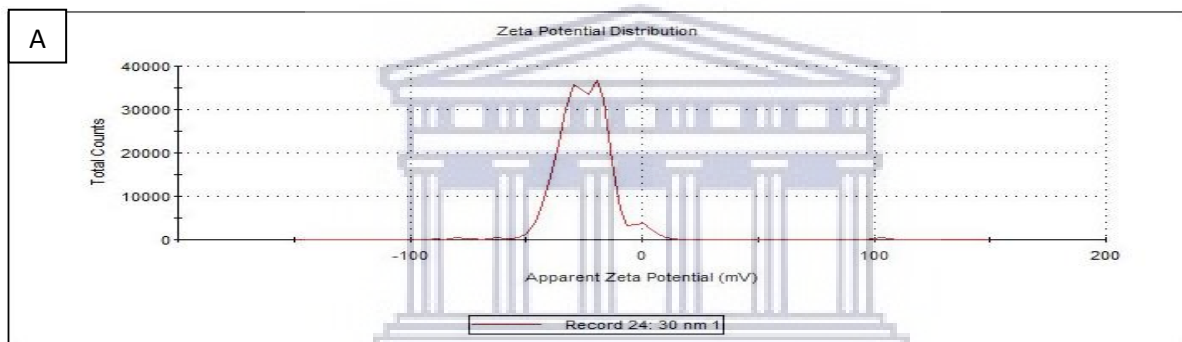


**Figure 3.1.2: Zeta Potential of AuNPs.** [A] 30 nm AuNPs (d.nm), [B] 50nm AuNPs (d.nm) and [C] 80 nm AuNPs (d.nm) at 25°C in in a dispersant of distilled water (dH<sub>2</sub>O).

According to Bhattacharjee (2016) all AuNPs used in this study are stable and negatively charged (78). The stability of AuNPs are dependent on ZP and AuNPs with a ZP less than +25 mV and greater than -25 mV are considered to have low degree of stability (75). As seen in Table 3 for 30 nm particles, the ZP is -23, 7 mV, 50 nm is -35, 7 mV and 80 nm is -29, 2 mV. This reveals that particles are moderately and highly stable. ZP is also crucial as it determines the initial absorption onto the cell membrane. AuNPs ZP between -10 mV and +10 mV are generally neutral, whereas ZP greater than +30 mV are considered strongly cationic and less than -30 mV are considered strongly anionic.

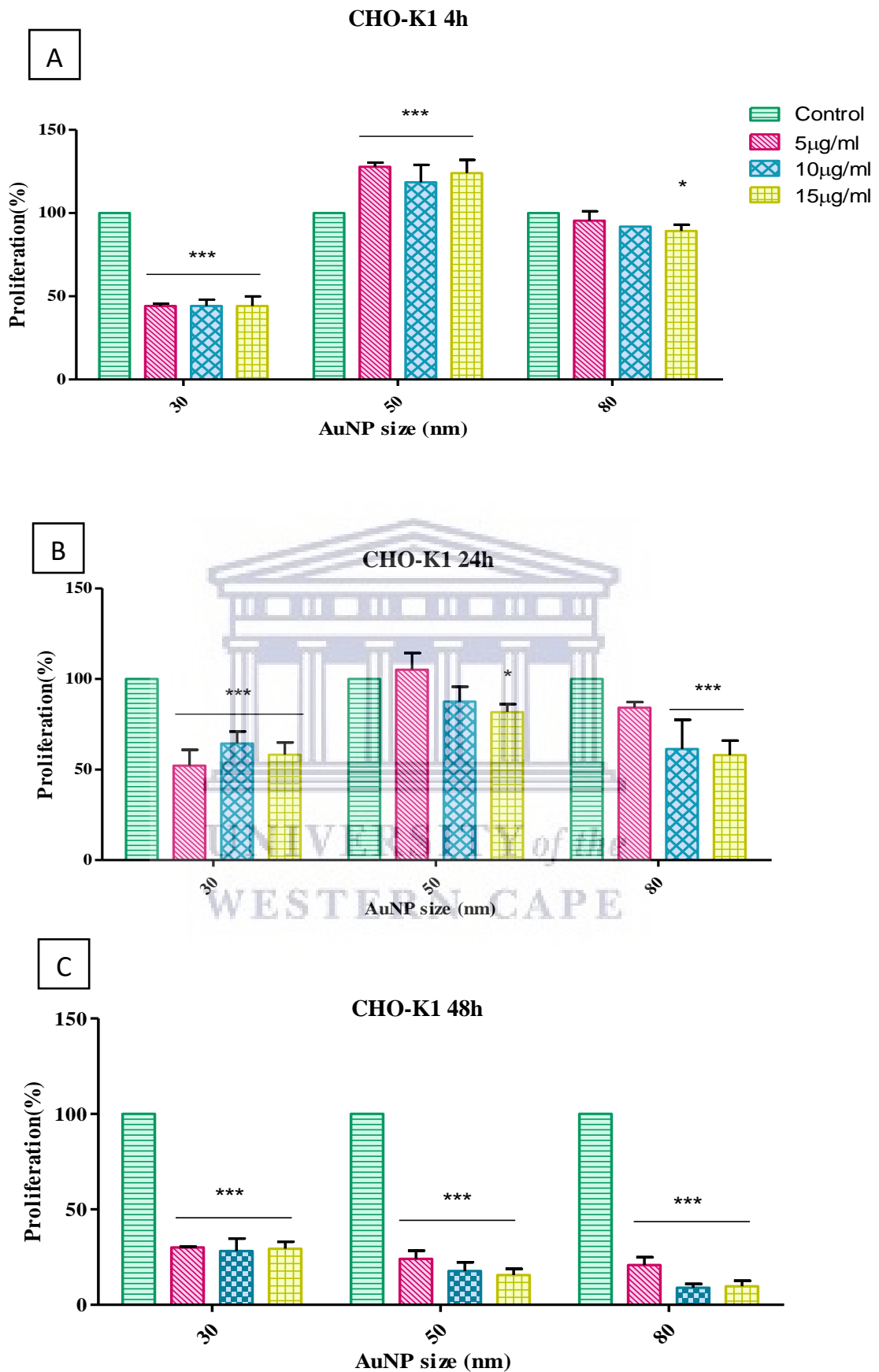
**Table 3:** Zeta potential and DLS analysis of AuNPs. Analysis of DLS represents the hydrodynamic size dispersity curves (samples are averaged) and ZP depicts the charge and stability of NPs. Values are graphically illustrated above.

<b>AuNP Sample</b>	<b>Zeta Potential (mV)</b>	<b>Dynamic Light Scattering (d.nm)</b>	<b>Polydispersity Index (PDI)</b>
<b>30</b>	-23.7	41.16	0.124
<b>50</b>	-35.7	48.24	0.282
<b>80</b>	-29.2	86.75	0.196

### 3.2. Cellular Proliferation and Viability

#### 3.2.1. Crystal Violet

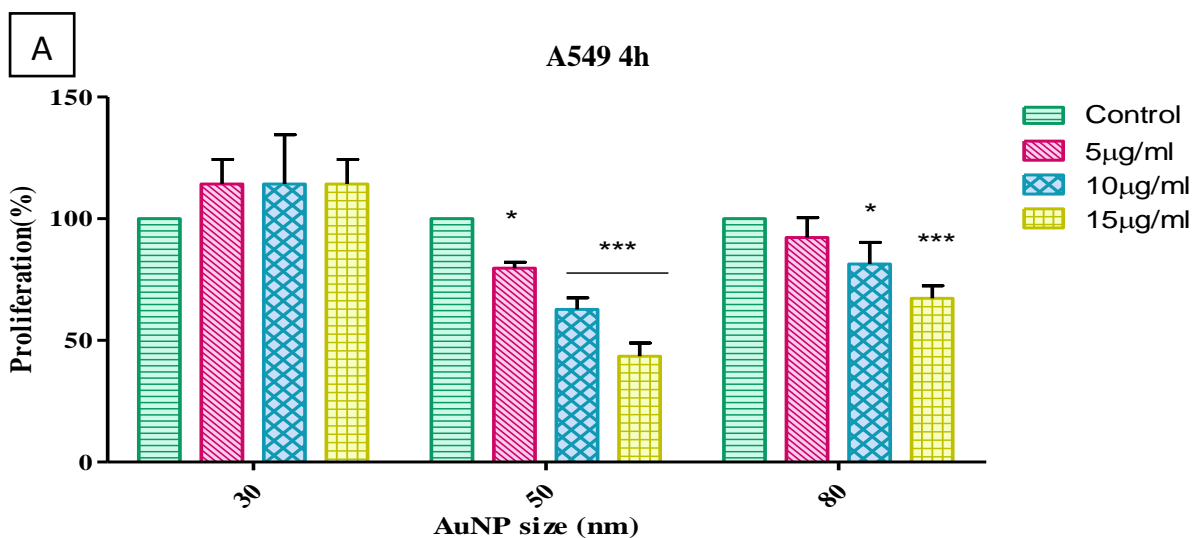
In order to determine impact various AuNP sizes and concentrations on the proliferation of A549 and CHOK1 cells, the crystal violet assay was utilized. Crystal violet is a triphenylmethane dye (4-[(4-dimethylaminophenyl)-phenyl-methyl]-N, N-dimethyl-aniline) which is commonly utilized to determine the cell number in monolayer cultures by assessing the absorbance of dye taken up by cells the cells (83). Crystal violet (CV) is an intercalating dye that enables the quantification of DNA which is always held proportional to the number of cells in the culture (83).



**Figure 3.2.1: The effects of AuNP size, concentration and exposure time on CHO-K1 cell proliferation.** [A] 4h post-treatment, [B] 24h post-treatment and [C] 48h post-treatment. \* p < 0.05, \*\*\* p < 0.001.

represents samples that are significantly different from the control set. \* ( $P < 0.05$ ), \*\* ( $P < 0.01$ ) and \*\*\* ( $P < 0.001$ ).

**Figure 3.2.1 [A]**-CHO-K1 cells treated for 4 hours demonstrated that 30 nm particles at all concentrations caused a significant ( $P < 0.001$ ) inhibition of cell proliferation when compared to the control. At 5, 10 and 15  $\mu\text{g/ml}$ , cell proliferation was reduced by 56%. In contrast, the 50 nm particles significantly stimulated proliferation across all concentrations with a 28%, 18% and 24% increase in cell proliferation, respectively. The 80 nm AuNPs decreased proliferation slightly at concentrations of 5 and 10  $\mu\text{g/ml}$ , but a significant ( $P < 0.05$ ) decrease in cell proliferation was only observed with the highest concentration. **[B]**-At 24h post-treatment, 30 nm AuNPs still inhibited CHO-K1 cell growth significantly ( $P < 0.001$ ) but to a lesser extent than that seen for the 4h treated samples. At the lowest concentration (5  $\mu\text{g/ml}$ ) a 48 % decrease was seen, whilst at 10 and 15  $\mu\text{g/ml}$  a decrease of 36% and 41% respectively, was observed. In the case of 50 nm particles, 10  $\mu\text{g/ml}$  caused a 5% increase in cell proliferation but, in contrast to the results in the 4 h samples, a significant reduction of 18%, was seen in the cells exposed to the highest concentration. At 10 and 15  $\mu\text{g/ml}$ , the 80 nm particles resulted in a significant decline in cell proliferation of 39% and 40%, respectively. **[C]**-After 48h, a significant ( $P < 0.001$ ) inhibition for all concentrations and all AuNP sizes, was observed. In the case of the 30 nm AuNPs, all concentrations 5, 10 and 15  $\mu\text{g/ml}$  decreased proliferation by approximately 70%. Cells exposed to the 50 nm particles displayed a dose-dependent decrease with the highest concentration (15  $\mu\text{g/ml}$ ) showing a decrease of 84%. Similarly with 80 nm particles, cell proliferation was significantly ( $P < 0.001$ ) reduced in comparison to the control with 5  $\mu\text{g/ml}$  (79, 2%), 10  $\mu\text{g/ml}$  (91.2%) and 15  $\mu\text{g/ml}$  showing a decrease of 90.3%.



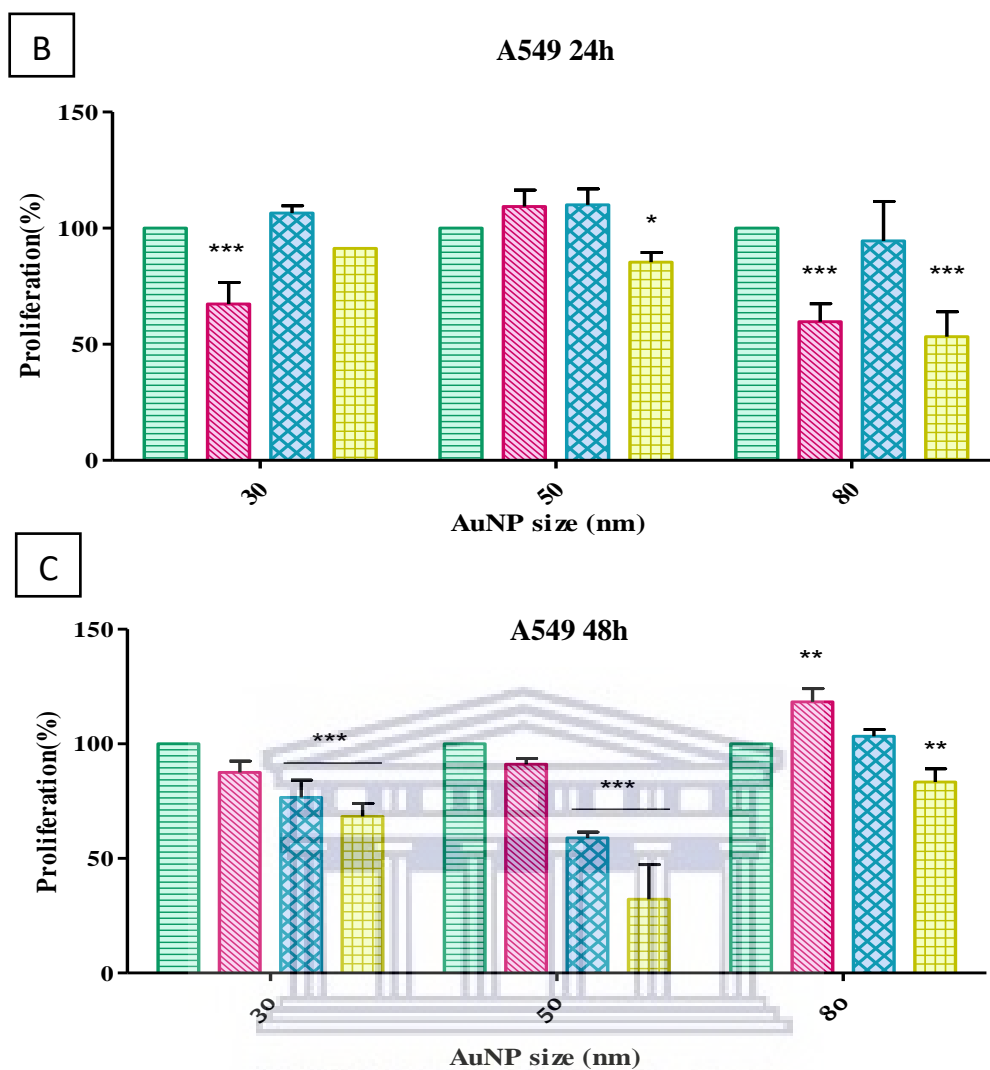


**Figure 3.2.2: The effects of AuNP size, concentration and exposure time on A549 cell proliferation.** [A] Cell proliferation 4h post-treatment, [B] 24h post-treatment and [C] 48h post-treatment. \* represents samples that are significantly different from the control set. \* (P<0.05), \*\* (P<0.01) and \*\*\* (P<0.001).

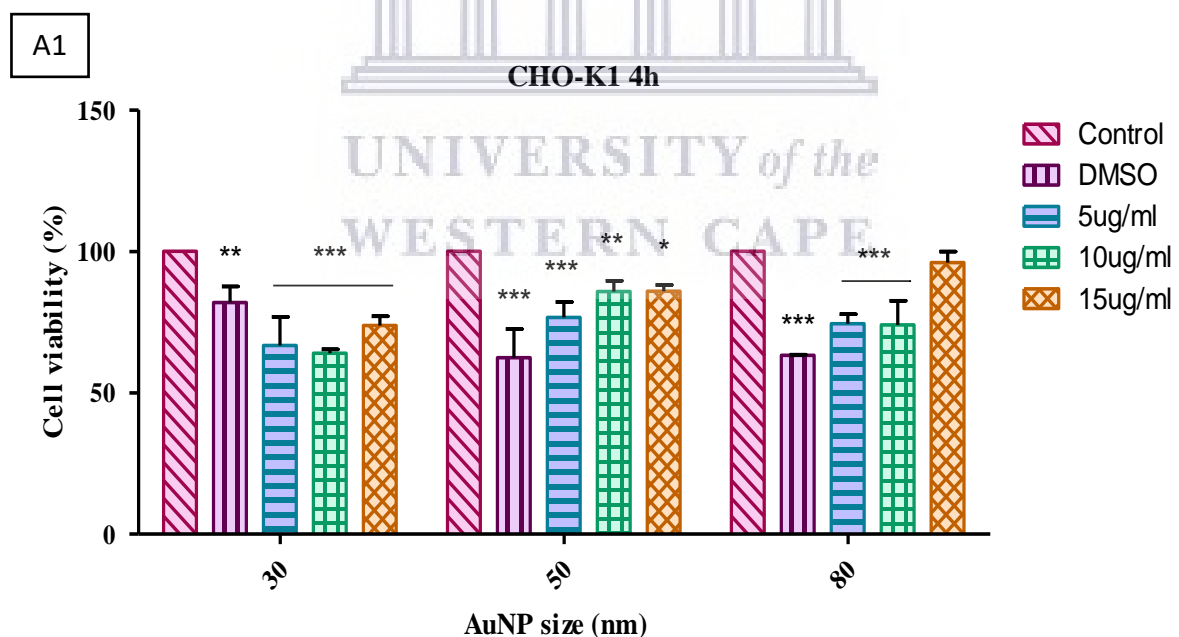
**Figure 3.2.2 [A]** 4h exposure: 30nm particles did not produce a statistical change in proliferation across all concentrations when compared to the control. The 50 nm AuNPs caused a significant dose-dependent decrease of 20%, 37% and 57%, respectively. 80 nm treated samples showed significant changes at the 10- and 15  $\mu\text{g/ml}$  with a 19% (P<0.05) and 33% (P<0.001) reduction in cell proliferation. **[B]**- After 24h, the 30 nm particles had a bi-phasic effect. At the lowest concentration, proliferation was decreased by 33%, while at 10  $\mu\text{g/ml}$  a 6% increase was observed, although not significant. 50nm AuNPs also had a non-statistical stimulatory effect at 5 and 10  $\mu\text{g/ml}$ . However, at the highest concentration a 15% reduction in the number of cells, was observed. Similar to the 30nm AuNPs, the 80 nm at 5  $\mu\text{g/ml}$

significantly decreased cell proliferation by 40% while the 10  $\mu\text{g/ml}$  treated cells did not differ significantly from the control. At the highest concentration, cell proliferation was down by 47%. [C]- After 48h of exposure, the 30 nm and 50 nm AuNPs had a dose-dependent decrease at 10 and 15  $\mu\text{g/ml}$  of - 23% and 32% for 30 nm and 41% and 68% for 50 nm. In the 80 nm particle samples, a significant increase of 18% and decrease of 17% was seen at the lowest and highest concentrations, respectively. The 80 nm AuNPs at 10  $\mu\text{g/ml}$  had no statistical effect on cell proliferation for both 24 and 48 h time periods confirming previous reports stating that size does matter.

Results for the 48h exposure time of the CHO-K1 cells revealed at least a 70% decrease in cell proliferation across all concentrations and all AuNP sizes. Due to CHO-K1 showing such insult after 48hrs, this time period was eliminated from further experimentation. This study aims to observe at which parameter cells are tolerant to treatment hence it was excluded.

### 3.2.2. Cellular Viability

The effects of AuNPs on CHOK1 and A549 cell proliferation obtained above was verified using the WST-1 assay. Cells were incubated at both 4h and 24h. Controls included untreated cells and a sample exposed to 10 % DMSO (positive control).



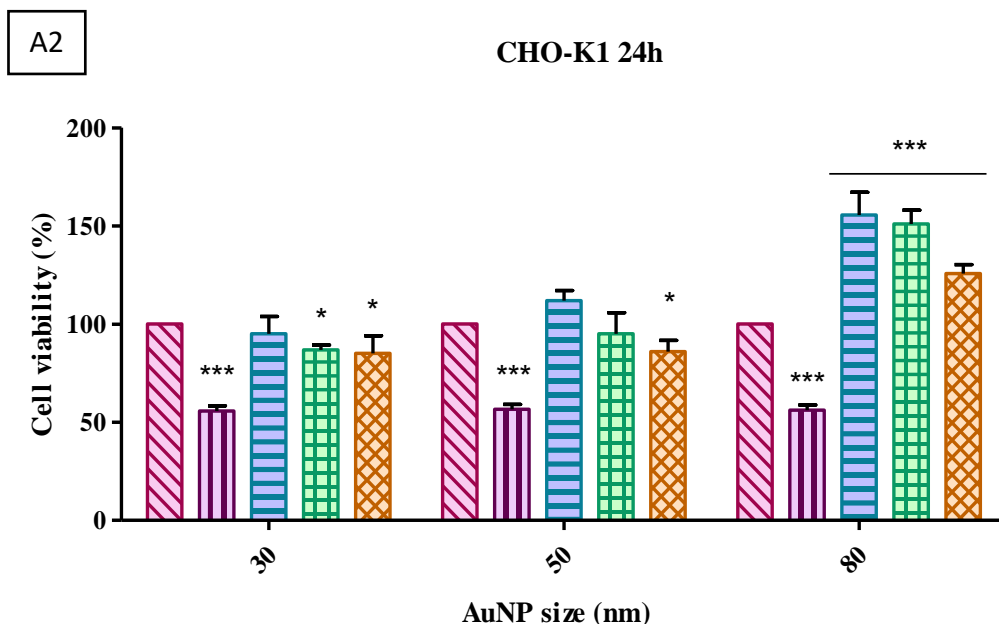


**Figure 3.2.3: Effects of AuNPs on CHOK1 cell viability.** Cell viability was measured after [A1]-CHOK1 4h exposure and [A2]-CHOK1 24h exposure to 5, 10 and 15 µg/ml. Significance is indicated with \* (P<0.05), \*\* (P<0.01) and \*\*\* (P<0.001)

**Figure 3.2.3** CHOK1 cells exposed to 10% DMSO showed a significant (P<0.001) decrease in the cellular viability in comparison to the control for both 4h and 24h providing the positive control of this assay. [A1] Similar to the crystal violet result, cell viability was significantly decreased in cells exposed to 30 nm particles at all concentrations for the 4h incubation. Cells exposed to 50 nm showed a decrease in viability of 23%, 14.3% and 14, 1% from lowest to highest concentration, respectively. The 80nm particles at 5 and 10 µg/ml caused a significant decrease in cell viability whilst at 15 µg/ml had no significant effect on cells after 4h. [A2] – 30 nm treated cells presented with a significant decrease in viability of 13% (10 µg/ml) and 5% (15 µg/ml). At 5- and 10 µg/ml for 50 nm, cells showed no significant changes in viability. However, at the highest concentration (15 µg/ml), a 14% decrease was seen. CHOK1 cells incubated with 80 nm particles showed a significant increase in cell viability compared to the control. An increase of 56%, 51% and 26% was observed at 5, 10 and 15 µg/ml, respectively. At 24h 80nm Au particles seemed to have a stimulatory effect whilst 30 and 50nm slightly inhibited cell viability at 10 and 15 µg/ml.

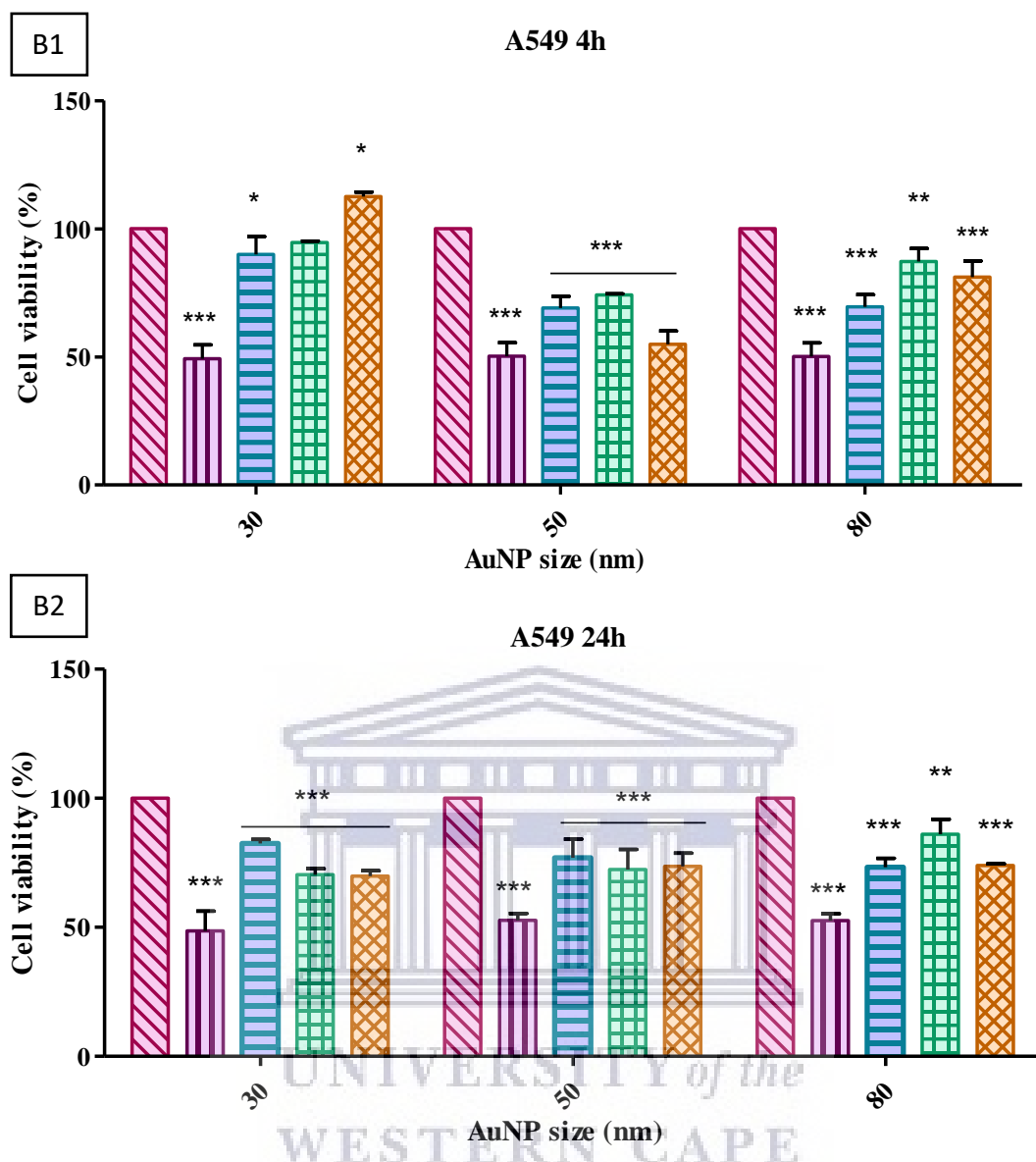


**Figure 3.2.4: Effects of AuNPs on A549 cellular viability.** Cell viability was measured after [B1]-A549 4h exposure and [B2] - A549 24 exposure to 5, 10 and 15 µg/ml. Significance is indicated with \* (P<0.05), \*\* (P<0.01) and \*\*\* (P<0.001).

A549 cells were similarly exposed to 10% DMSO and a significant decrease in viability, as with the CHO-K1 cells, was observed. **[B1]** - A significant decline in cell viability of 10% and 13%, respectively, was seen for 30 nm particles after 4h at 5 and 15 µg/ml. In the case of 50nm treated cells a significant (P<0.001) reduction in viability was observed across all concentrations. Similarly to 50nm, the 80 nm treatment displayed a significant decrease in cell viability at all concentrations. The decrease percentage was 30%, 13% and 19% from the lowest to the highest concentration. **[B2]** - After 24h, cells exposed to 30 nm revealed a significant dose-dependent reduction in cell viability. 50nm treatment revealed similar results to that of 30nm with a significant decline in cell viability across all concentrations with all

concentrations reducing viability by approximately 26%. A549 cells treated with 80nm colloidal gold resulted in a significant decline in cell viability of 26, 7%, 14% and 26, 1% at 5, 10 and 15  $\mu\text{g/ml}$ , respectively compared to the control.



UNIVERSITY *of the*  
WESTERN CAPE

### 3.3. Oxidative Stress

The effects of AuNPs on the production of reactive oxygen species (ROS) was measured using the DCF-DA fluorescent assay and a fluorescent plate reader.

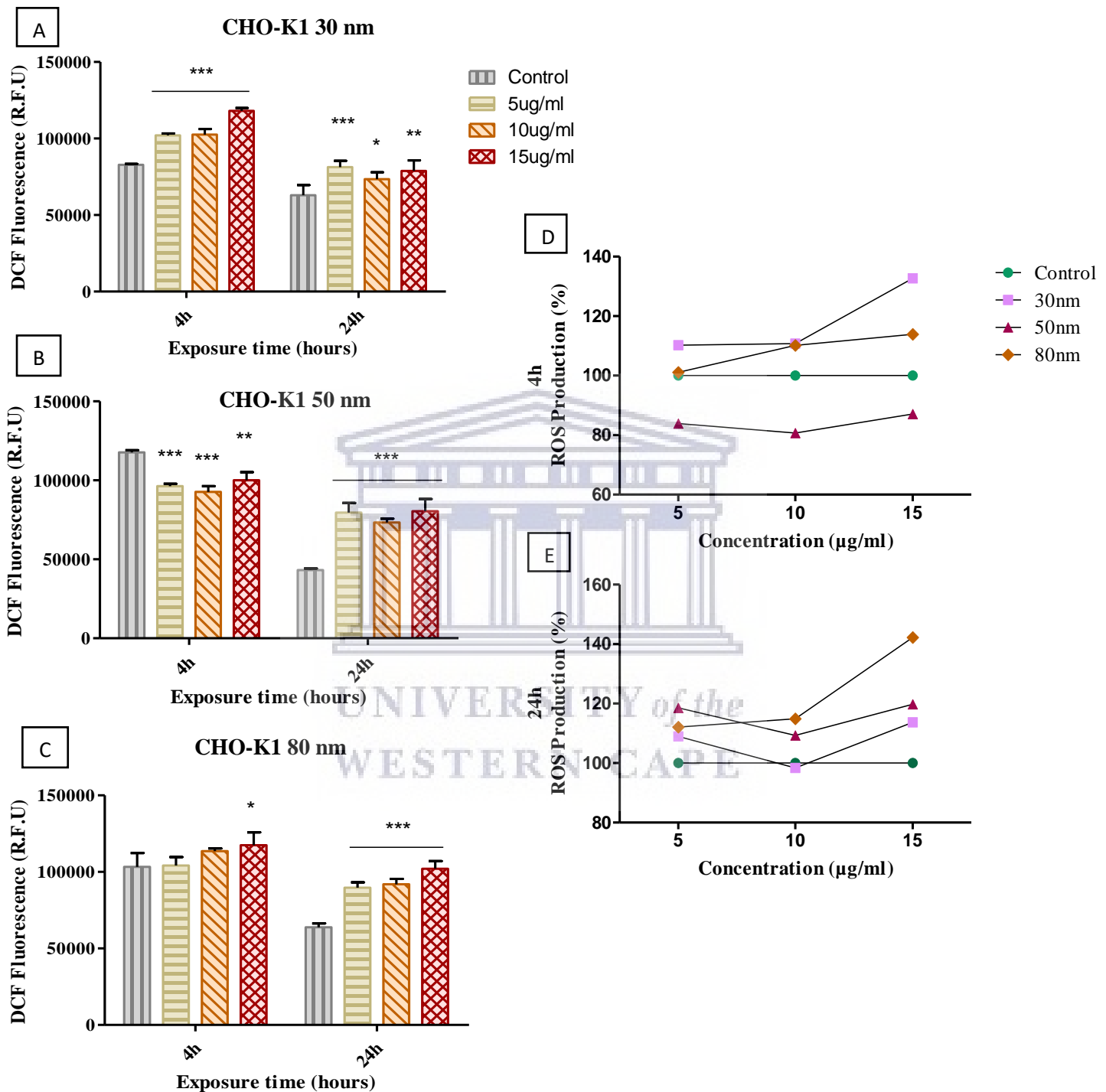


**Figure 3.3. 1: Detection of ROS production in CHOK1 cells.** Using DCFDA after exposure to AuNPs (5, 10 and 15 µg/ml). Samples are shown relative to control (untreated samples) over 4 and 24 hours. [A] – 30nm, [B] – 50nm, [C] – 80nm, [D] – (all sizes) 4h, [E] – (all sizes) 24h. Significance is indicated with \* (P<0.05), \*\* (P<0.01) and \*\*\* (P<0.001). ?

**Figure 3.3.1.** [A] – 30 nm treated samples showed a significant dose-dependent increase in fluorescence of 102052, 102588 and 118036 rfu at 5,10 and 15 µg/ml after 4h incubation, respectively. With 15 µg/ml showing the most prominent increase in ROS production. After 24h exposure, samples still presented with significantly increased ROS levels with the lowest concentration (5 µg/ml) inducing the highest ROS production, at 18421,2 rfu greater than the control sample (10 000 rfu). [B] – At 4h exposure to 50 nm particles the 5, 10 and 15 µg/ml treatments significantly decreased ROS levels in comparison to the control sample. However, after 24 hour treatment the 50 nm AuNPs had the opposite effect and induced a highly significant increase in ROS levels for all concentrations. [C]- At 4h exposure a significant increase in ROS was observed at 15 µg/ml (80 nm) of 14 208 rfu. However, after 24h, all concentrations of the 80 nm particles caused a statistically significant ( $P<0.0001$ ) increase in the production of ROS. [D] & [E] represents the production of ROS across the different AuNP sizes. After 4h exposure, 50nm produced less ROS then the control sample whilst the 30nm treatment at 15 µg/ml showed the highest ROS production. After 24h, 80nm treatment caused an outspoken increase in ROS levels whilst cells treated with 30 nm particles showed a decrease in ROS. The 50nm particles also increased ROS, but not to the extent that the high concentrations of the 80 nm AuNPs did.

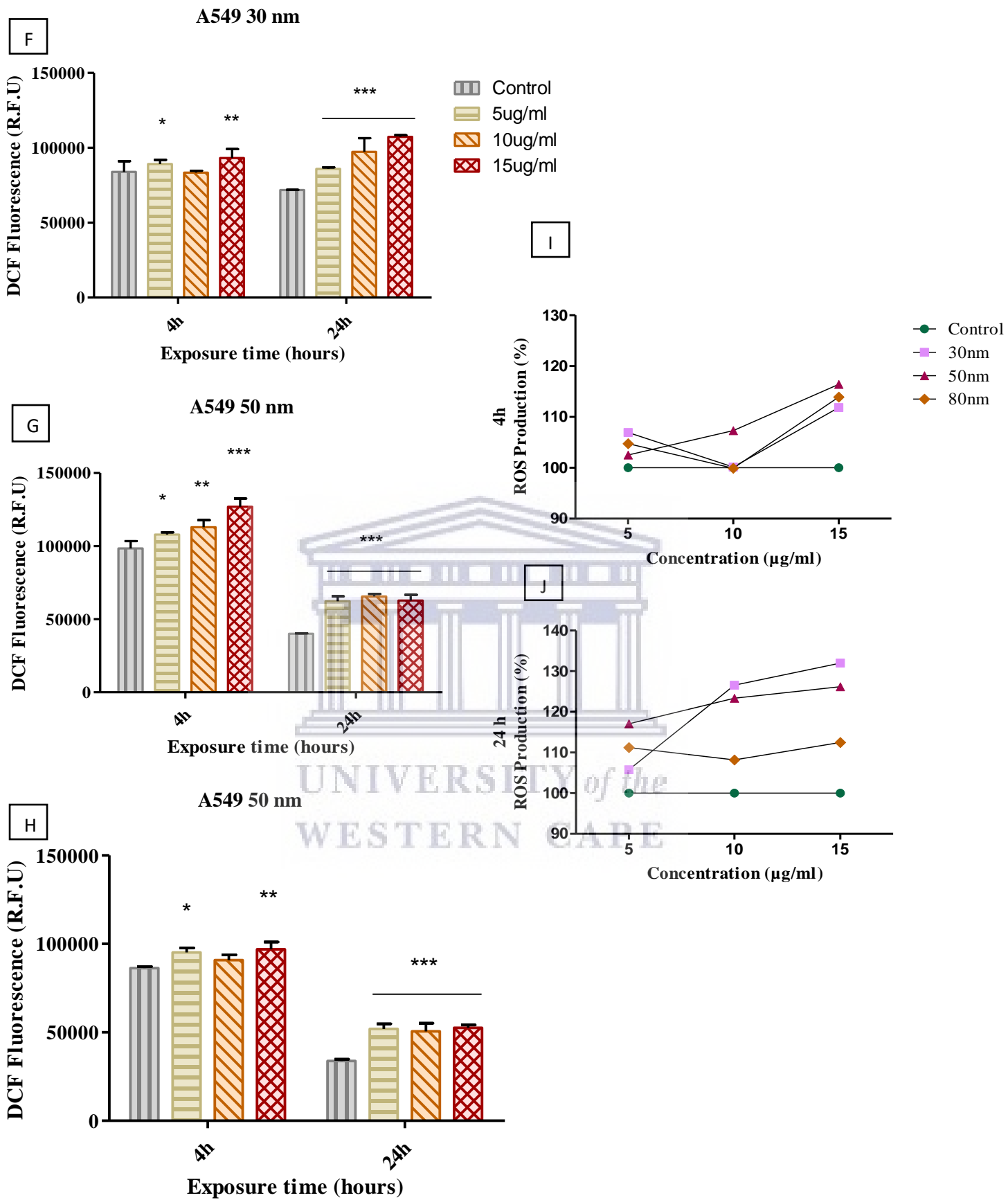
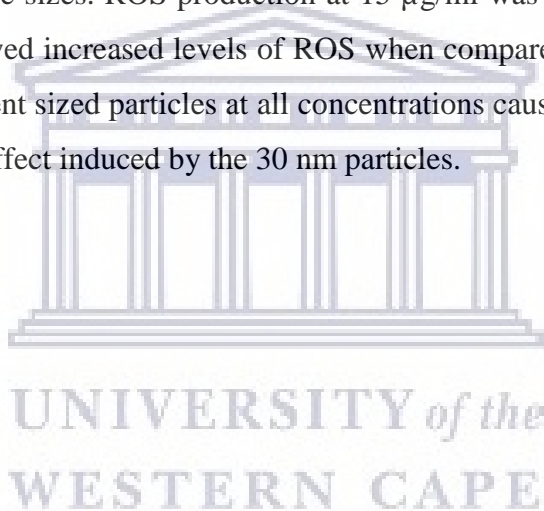


**Figure 3.3.2: Detection of ROS production in A549 cells.** Using DCFDA after exposure to AuNPs (5, 10 and 15 µg/ml). Sample significance are relative to the control (untreated samples)

over 4 and 24 hours. [F] – 30nm, [G] – 50nm, [H] –80nm, [I] – (all sizes) 4h, [J] – (all sizes) 24h. Significance is indicated with \* (P<0.05), \*\* (P<0.01) and \*\*\* (P<0.001).

**Figure 3.3.2 [F]** - A549 cells exposed to 30nm for 4h showed significant increase in ROS production compared to the control at 5 and 15 µg/ml by 9228, 8 and 13296, 1 rfu, respectively where at 10 µg/ml no significant effects were observed. At 24h all concentrations displayed a significant (P<0.001) increase in fluorescence thus ROS formation. **[G]**- Cells exposed to 50nm for 4h has a dose dependent increase in ROS production of 9494,3, 14545,3 and 28481,3 rfu, with the highest levels of ROS at 15 µg/ml treated samples. After 24h, all concentrations induced a significant (P<0.001) increase in ROS production. **[H]**- Samples exposed to 80 nm particles showed a significant increase in ROS production at 5 and 15 µg/ml. At 24h, all concentrations significantly increased ROS. **[I]**- 50nm exposure at 4h had the highest ROS production among the three sizes. ROS production at 15 µg/ml was the highest for all sizes. 30nm and 80nm also showed increased levels of ROS when compared to the control sample. After 24h, the three different sized particles at all concentrations caused a significant increase in ROS with the greatest effect induced by the 30 nm particles.



### 3.4. Cell death detection using Hoechst and Acridine Orange Fluorescent Staining

A dual staining (Hoechst/acridine orange) fluorescent microscopy method was employed to visualise autophagy and the effect of AuNPs on morphology and possible apoptosis induction. Hoechst 33342 is capable of penetrating intact cell membranes of viable cells and cells undergoing apoptosis and stains the DNA. Acridine orange is a lysosomotropic fluorescent compound that serves as a tracer for acidic vesicular organelles including autophagic vacuoles and lysosomes (92). Cells undergoing autophagy has an increased tendency for acridine orange staining when compared to viable cells, however acridine orange is not a specific marker for autophagy and therefore other techniques are needed to verify the appearance of increased autophagic activity.

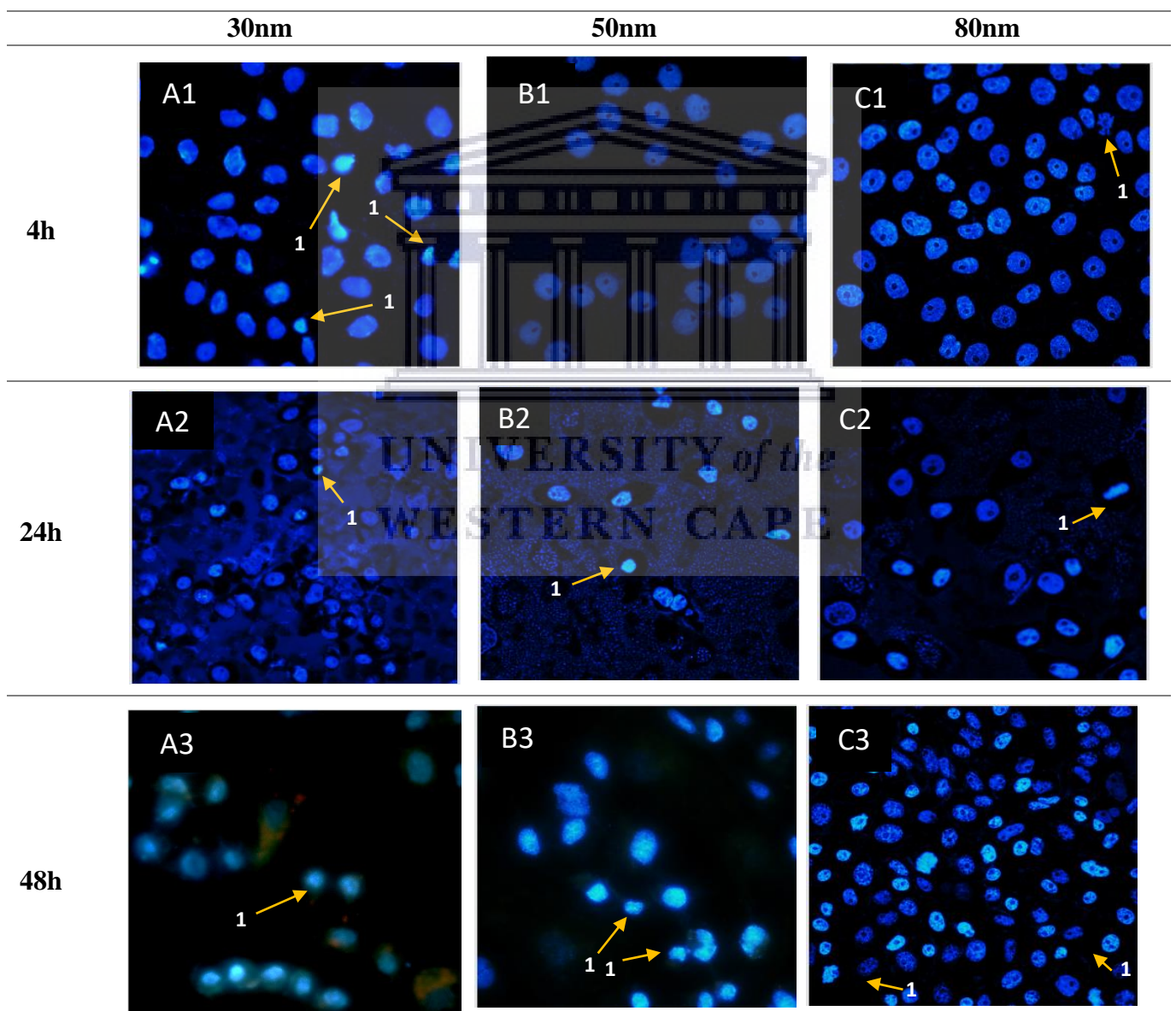


**Figure 3.4.1: Morphological changes of selected CHO-K1 cells as shown with either Hoechst alone or with a dual stain of Hoechst 33342 and acridine orange.** Cells were treated with various concentrations and sizes of AuNPs and were imaged via fluorescent microscopy using the FITCI filter (40X). **Arrows indicate:** (1) Apoptotic nuclei (some bright/intensely stained nuclei indicate apoptosis). [A1]-15 µg/ml, [A2]-10 µg/ml, [A3] - 10 µg/ml (dual stain), [B1]-5 µg/ml, [B2]-10 µg/ml, [B3] - 15 µg/ml, [C1] - 10 µg/ml, [C2] - 5 µg/ml and [C3]-10 µg/ml.

CHOK1 cells were treated with 30, 50 and 80 nm AuNPs at 5, 10 and 15 µg/ml. Cells were then dual stained with Hoechst 33342 and AO and observed under 20X and 40X magnification. Figure 3.2.1 [A1] - Some apoptotic nuclei was observed at 15 µg/ml. [A2] - displayed apoptotic formation with most nuclei presenting as normal. [A3]- Nuclei were surrounded by red/orange structures indicative of pH change, this may be due to autophagic vacuoles and or the presence of lysosomes. [B1]-Compared to 30nm and 80nm showed a slight decrease in cell density. [B2] Apoptosis was present as nuclei displayed a change in morphology and [B3] – showing more apoptotic nuclei than 4h and 24h. [C1]& [C2] - both showed apoptosis whilst [C3] - presented with most induced apoptosis. At 24h exposure (CHOK1) background staining was heavily present. This may have been due to inadequate washing or not allowing enough drying time. However, nuclei are clearly presented.

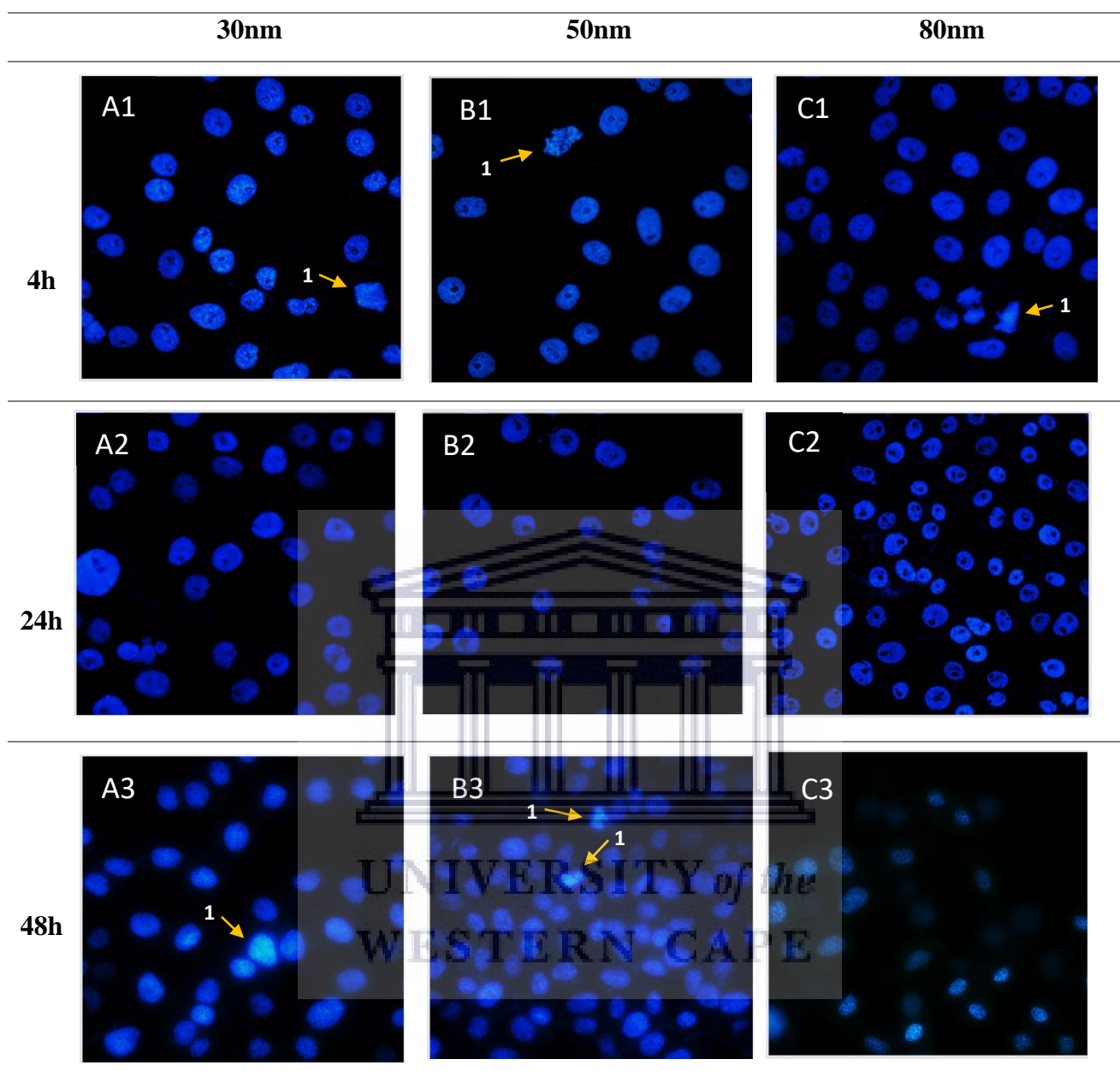


**Figure 3.4.2: Morphological changes of selected A549 cells as shown with either Hoechst alone or with a dual stain of Hoechst 33342 and acridine orange. Cells were treated with various concentration and sizes of AuNPs and were imaged via fluorescent microscopy using the FITCI filter (40X). Arrows indicate: (1) Apoptotic nuclei. [A1]-15  $\mu\text{g/ml}$ , [A2]-5  $\mu\text{g/ml}$ , [A3] - 5  $\mu\text{g/ml}$ , [B1]-10  $\mu\text{g/ml}$ , [B2]-5  $\mu\text{g/ml}$ , [B3] - 5-  $\mu\text{g/ml}$ , [C1] - 15  $\mu\text{g/ml}$ , [C2] - 5  $\mu\text{g/ml}$  and [C3]-15  $\mu\text{g/ml}$ .**

In A549 cells Figure 3.2.2 [A1], [A2] and [A3] all showed fairly consistent cell density with 4h and 48h showing apoptosis, however not much. [B1]& [B2] displayed a decrease in cell density whilst [B3] - Apoptosis was present at 5  $\mu\text{g/ml}$ . [C1]- Apoptosis was seen indicated by the change in morphology along with nuclei undergoing mitotic division (anaphase) this was indicated by the finger-like projections and segregation of the chromosomes. [C2]-Nuclei did show a change in structure however majority appear health. [C3] – A decrease in cell density was seen and nuclei seem to have varying fluorescent intensity

As observed in the viability and proliferation assay the A549 cells seem to be more tolerant to AuNP treatment at different time periods in comparison to CHOK1 cells. Although A549 cells also present with apoptosis, it is not as frequent as in CHOK1 cells.



## CHAPTER 4: DISCUSSION

---

Nanoparticles, typically 10 – 1000 nm in diameter, have potential in chemistry, engineering, biology, and medicine (34).

According to the World Health Organization (2020), in 2018 cancer accounted for an estimated 9.6 million deaths, with lung cancer being the most frequently diagnosed. Additionally, Newhauser *et al* (2015) reported that 50% of patients receive radiotherapy as treatment, however the high incidence of treatment-related illness in cancer survivors such as additional cancers, cardiovascular diseases and fertility problems are alarming (93). Furthermore, radio resistance is inherent of tumour cells and remains an unsolved problem (94). Significant effort has been devoted to the use of gold nanomaterials with distinct physical, chemical, and biological properties for use in nanomedicine.

With substantial advances observed in the field of diagnosis, treatment, disease prevention, preserving and improving human health, researchers are becoming more optimistic regarding the development of novel strategies to address biological issues (95). AuNPs exhibit good biocompatibility and controlled bio-distribution patterns which make them an ideal candidate for the basis of innovative therapies (96). In addition, the technological improvements in radiation therapy has led to an increased interest to implement gold-based nanomaterial as radiosensitizer. Their radiation sensitization potential could be attributed to their high mass energy absorption linked to their high atomic number (97). By combining radiation with AuNPs, an advantage has been seen in dosing capabilities and improved tumour control (62,98).

The main aspect of this study was to explore the *in vitro* cytotoxic effects of various AuNPs on a normal cell line, (CHO-K1) and a lung cancer cell line (A549). The aim is to determine the optimal time, dose, and ideal size of the AuNP that has the least adverse effect on cell viability to develop a non-toxic AuNP probe than can be employed *in vivo* and eventually in a clinical setting. AuNPs have been known to exhibit great potential as radiosensitizer, the strategy is to prime the cells with the optimal AuNP for a specific time and irradiate the cells inducing damage to the AuNP treated cells whilst limiting the dose to the surrounding (healthy) tissue, thus, yielding a greater therapeutic effect (99).

## 4.1. AuNP characterisation

For this baseline study, commercially purchased AuNPs, were used. The stability of AuNPs plays a major role in their application and can be controlled by various methods such as increasing electrolyte concentrations, adjusting the solution pH, adding different inorganic salts, etc. (100). AuNPs were coated with citrate ions by Sigma-Aldrich (Johannesburg South-Africa) causing a reduction in gold ions to atoms for stabilization (101). The citrate acts as a protective agent via electrostatic repulsion and prevent agglomeration of the metal nanostructures (100). Characterization via DLS and ZP were performed to obtain conclusive results on size and surface charge, since the properties of AuNPs play a significant role in their interaction with the cells.

### 4.1.1. Dynamic Light Scattering

The citrate stabilized commercially purchased AuNPs were characterized for both size distribution and stability. DLS characterization revealed larger particle sizes than the purchased AuNP size. 30 nm particles measured 11, 16 d.nm greater, 50 nm at 18, 24 d.nm smaller and 80 nm at 6, 75 d.nm greater than the core size. The larger measured sizes may be due to the hydrodynamic radius ( $R_H$ ), the hydrodynamic radius is a hypothetical hard sphere which diffuses with equal speed as the measured particle (78). In most cases when distributed particles are hydrated or solvated the surface of the NP is changed dependent on the adsorbed layer, the particle surface absorbs proteins, forming a protein corona (78). This corona is characterized by a soft and hard component, the soft corona is a loose layer found above the hard corona made up of molecules with various sizes and charges (102). The hard corona is the inner stable layer closely bound to surface particles (103). Smaller particles tend to aggregate and thus displaying higher  $R_H$  (78) this can clearly be seen with the 30nm particle. 50 nm particles however showed a decrease in size this could be explained by Nobbmann *et al* (2016) the smaller size measurement can be is due to electrostatic interactions: particles caught in a confined space, bounces off equally-charged neighbours with higher speed than when freely diffusing, thus the faster movement of particles are measured as a smaller apparent size (104). The poly dispersity index (PDI) describes the degree on non-uniformity of a size distribution of particles (105). All samples (30, 50 and 80 nm) were found to be moderately polydispersed with values less than <0.4 yet greater than 0.1.

#### 4.1.2. Zeta Potential (ZP) determining surface charge of the AuNPs:

ZP analysis provides useful information regarding the stability of colloidal AuNPs, it also provides information about whether NPs are positively or negatively charged, which play an important role in their properties and functions (27). Goodman *et al* (2004), showed that positively charged (cationic) AuNPs showed moderate toxic effects whilst negatively charged (anionic) AuNPs was non-toxic (38). NP-mixtures are classified as  $\pm 0-10$  mV,  $\pm 10-20$  mV,  $\pm 20-30$  mV and  $\pm 30$  mV: highly unstable, fairly stable, moderately stable and highly stable, respectively (78). ZP analysis revealed that 30, 50, and 80 nm AuNPs have a surface charge of -23.7, -35.7, and -29.2 mV, respectively. This reveals that all samples are anionic, with 30 nm and 80 nm being moderately stable and 50 nm highly stable as seen in **Table 3**, the negative charge is attributed to the citrate-buffer ensuring good NP stabilization (106).

AuNPs uptake by cells occur via two steps, first binding to the cell membrane and then secondly, the internalization of AuNPs into the cell, which occur via receptor mediated endocytosis (107). The binding to the cell membrane is mostly affected by the surface charge of NPs (108). Honary and Zahir (2013) reported that NPs with a higher surface charge bound strongly to the cell membrane and show a higher cellular uptake (109). In other studies, the 50 nm AuNP stabilized in citrate had a negative charge, as well as have the highest cellular uptake by cells, when compared to other AuNP sizes (63). The high negative charge of AuNPs also aids in stabilization and prevents aggregation. Cellular growth media contains serum proteins, amino acids, vitamins, electrolytes, and other chemicals which could interact with the NPs and change their aggregation state and other physiochemical properties (110). However, NPs in an aqueous solution aids in surface charge stabilization and prevents aggregation via electrostatic repulsion (111). Wang *et al* (2016) investigated the best method for running ZP and concluded that water was the best medium to ensure good data reliability (112). As mentioned in *section 2.1.1.*, AuNPs characteristics were carried out in water and therefore the data can be considered accurate.

#### 4.2. Cell Proliferation

AuNPs are generally considered highly biocompatible due to their inert nature (113,114) nevertheless literature reported the cytotoxic effects of AuNPs on cells (115,116). Studies suggested that AuNPs toxicity is dependent on size, shape, surface charge, coating, concentration and cell line. (51,117). The crystal violet assay evaluated the cell proliferation of CHO-K1 and A549 cells after exposure to different AuNP parameters to establish the overall cytotoxicity, as the molecular interactions of AuNPs in cells remain largely unexplored.

As seen in this particular study, CHOK1 cells are extremely sensitive to 30 nm gold particles at all concentrations at all exposure times, indicating that 30 nm is not ideal in this particular cell line as it results in the most outspoken cytotoxic effect. At 4h cell proliferation was decreased by 56% across all concentrations and similar results were displayed for both 24 and 48h. A study by Vechia *et al* (2020) reported that 30nm particles showed high cytotoxicity in NIH3T3 cells when compared to other AuNP particle sizes, the study attributed this toxicity to the accumulation of particles within the cells (106). Additionally Coradeghini *et al* (2013) reported that the size and the internalization of AuNPs are crucial factors when assessing the toxicity of NPs (118). Vechia *et al* (2020) continued to report that 30 nm particles displayed toxicity in both HeLa and B16F10 cells however, AuNP treatment seemed to have a greater effect on HeLa cells, thus demonstrating that sensitivity to AuNPs differ across cell lines. This was shown by Chueh *et al* (2014) where the effects of AuNPs were investigated on various mammalian cell PK-15, Vero, NIH3T3 and MRC5 demonstrating a variation across cells in response to the same treatment (35). On the contrary, as seen in Figure 3.2.1. 50 nm particles induced a significant ( $P<0.001$ ) increase of 28%, 19% and 24% in CHOK1 cell proliferation after 4h of exposure at 5,10 and 15  $\mu\text{g/ml}$ , respectively. A recent study indicated that 18 nm AuNPs have the ability to penetrate cells, yet not result in toxicity (37). Chithrani *et al* (2006) reported that maximum uptake into HeLa cells occurred at 50 nm AuNPs when compared to 14 and 74 nm particles (58). Similarly, Yue *et al* (2018) revealed after 24h treatment, 50 nm gold nanoparticles had the greatest cellular uptake in U87 cells. Both studies reported that although maximum cellular uptake occurred at 50 nm no cytotoxicity was observed, cell proliferation was at 98 % and greater than 80%, respectively (58,119). Research shows that certain AuNP sizes and concentrations may increase cellular proliferation and that toxicity of the NP is time-, size-, and concentration-dependent. After 24h, 50 nm AuNPs induced a dose-dependent effect in CHO-K1 cells. 50 nm AuNPs revealed a 5% increase in cell proliferation compared to the control with only 15  $\mu\text{g/ml}$  having a significant ( $P<0.05$ ) decrease in proliferation. This result was also observed by Lu *et al* (2010) that found low concentrations of AuNPs may stimulate proliferation and at higher concentrations may result in loss of swollen mitochondria and chromatin condensation resulting in a toxic effect (120). Li *et el* (2016) found that 60 nm AuNPs resulted in efficiently increasing proliferation in Human Periodontal Ligament Stem Cells (hPDLCS) when compared to 20, 40 and 80 nm (8). The finding in Figure 3.2.1 [A] coincide with these, as observed 50 nm AuNPs increased cell proliferation by 28 %, 19% and 24 % at 5, 10 and 15  $\mu\text{g/ml}$ . Whilst at 30 and 80 nm AuNPs showed significant decreases at 15 $\mu\text{g/ml}$  after 4 h and at both 10 and 15  $\mu\text{g/ml}$  after 24 h, the lowest concentration

showed to have no effect on cell proliferation however at both 4h and 24h a dose-dependent decrease in cell proliferation was seen thus presenting that AuNPs smaller and larger than 50nm resulted in the inhibition of proliferation thus in agreeance with the previously mentioned studies. At 48 h of exposure CHOK1 cells revealed that at all AuNP sizes 30, 50 and 80 nm across all concentrations 5, 10 and 15  $\mu\text{g/ml}$  had a significant ( $P<0.001$ ) decrease in cell proliferation. It can thus be said that the duration of exposure played a major part in the toxicity. Thus when comparing 30 nm, 50 nm and 80nm AuNPs it is clear that the smallest AuNP size produced the greater cytotoxic effect. This may be due numerous factors such as smaller particles being endocytosed by cells and aggregating (121).

Cell proliferation in A549 cells were increased after treatment with 30 nm after 4h, although not significant an increase was observed. These results correspond with that of Liu *et al* (2014) where AuNPs (20 and 40nm) induced stimulation of A549 proliferation. The study indicated that smaller particles resulted in cytotoxicity due to the ability to penetrate cells and cellular compartments. Based on the finding the study alluded that AuNP treatment showed a strong size and cell type-dependency (122). 50 nm particles showed a significant dose-dependent decrease in proliferation of 20, 4%, 37, 3% and 56, 5% at 5, 10 and 15  $\mu\text{g/ml}$  after 4h treatment. Similarly, 80 nm showed a significant cytotoxic effect at the higher concentrations of 10 and 15  $\mu\text{g/ml}$ . As mentioned above this corresponds with Lu *et al* (2010) that higher concentrations may result in adverse cellular effects (120).

After 24h A549 cells revealed a significant decrease at 5  $\mu\text{g/ml}$  for both 30 nm and 80 nm AuNPs. This contradicts literature, that lower concentrations are less toxic compared to higher concentrations (120). As mentioned by Liu *et al* (2014) A549 cells displayed an increase in proliferation even after 48h, the results, at 48h A549 cells showed a dose-dependent decrease in cell proliferation. However, compared to 30 nm treatment, the cells seem to be affected to a greater extent. Thus when comparing the effects of AuNP sizes and concentrations on A549 cells, 50 nm and 80 nm AuNP treatment at 15  $\mu\text{g/ml}$  (for all exposure times) showed the most significant cytotoxic effects (Figure 3.2.2). Sun *et al* (2019) did an investigation on the anti-cancerous effects of ~50 nm AuNPs on A549 cells. It was reported that cell death was concentration-dependent and the IC<sub>50</sub> found at 15  $\mu\text{g/ml}$ , (123). Research showed that certain sizes and concentrations of AuNPs have promoting effects on cell proliferation as seen with the 50 nm AuNP in the CHO-K1 cell line and that cytotoxicity of AuNPs is size-, concentration-, and time-dependent (8).

### 4.3. Cell Viability

The WST-1 assay was utilized to determine the effects of AuNPs on cellular viability. WST-1 was employed to confirm the proliferation results obtained from the CV assay.

CHOK1 cells treated with 30 nm particles for 4h showed a significant decrease in cellular viability for all concentrations. This indicated the amount of metabolically active cells were reduced at all concentrations compared to the untreated samples. After 24h, 30 nm AuNPs caused a significant decrease at 10 and 15  $\mu\text{g/ml}$  ( $P < 0.05$ ). The lowest concentration seemed to have no effect. These findings coincide with cell proliferation results that at 30 nm AuNPs caused a significant decrease in cell proliferation and displayed increased cytotoxicity. CHOK1 cells treated with larger particles, 50 and 80nm, revealed a decrease in cell viability. After 4h at 50nm all concentrations displayed an inhibitory effect whilst for 80nm only 5 and 10  $\mu\text{g/ml}$  showed a significant decrease in cell viability. However, after 24h of treatment 50 and 80 nm treated cells indicated an increase in cell viability for 50 nm at 5 and 10  $\mu\text{g/ml}$  and for 80nm at all concentrations.

A549 cells treated with 30 nm particles for 4h revealed at 5  $\mu\text{g/ml}$  a significant decline of 10% and at 15  $\mu\text{g/ml}$  a significant increase in viability of 13%. However, after 24h all concentrations had a significant ( $P < 0.001$ ) decreasing effect on cell viability. When treated with 50 nm particles, A549 cells for both 4h and 24h showed significant ( $P < 0.001$ ) reduction in cell viability. Additionally, 80nm treated cells presented a significant reduction across all concentrations after both 4h and 24h. Rosli *et al* (2015) described that 50nm AuNPs resulted in high levels of toxicity compared to 13 nm and 70 nm particles in MCF-7 cells. The study indicated that the level of toxicity caused by 50 nm particles was due to the rate and extent of AuNP uptake. According to literature AuNPs enter the cells via receptor mediated endocytosis faster and more efficiently compared to other particles of a simpler size (58). The reason for this is theoretically based on the wrapping effect, this effect describes how the cell membrane encloses the AuNP. The factors that play a vital role in how fast and how much particles are taken up is the free energy from ligand-receptor interaction and the receptor diffusion kinetics on the sites of the cellular membrane. The study confirmed that toxicity was found at higher concentrations and this phenomenon is explained by the fact that lower concentrations of AuNPs possess less AuNP in solution resulting in lower ligand-receptor binding whilst at higher concentrations more AuNPs are present, leading to faster and more abundant binding thus shorter wrapping time and more effective uptake (124). Investigation of how the AuNPs are taken up by the cell was not examined, however as mentioned above, research indicate that

AuNPs with a diameter between 40-60 nm have the best cellular uptake efficiency via endocytosis (122). These findings correlate with that in this study, that at 50 nm, significant toxicity in A549 cells is observed. Although cytotoxicity is also seen at higher (80nm) and lower (30nm) sizes, the 50 nm particles caused higher levels of cytotoxicity. This may indicate that in A549 cells, maximum uptake occurred at this particular size, with emphasis on the high concentration of 15 µg/ml. In contrast to the lung cancer cell (A549), the 50 nm AuNPs increased cell proliferation in the normal CHOK1 cells (Fig.3.2.1B). After 4 hours, the 5 µg/ml AuNP had a stimulatory effect with an 8.8% upsurge in cell proliferation when compared to the control. At 10- and 15 µg/ml AuNPs, only a 0.4% reduction in cell proliferation was observed in the CHO-K1 cells.

Various AuNP sizes are taken up differently by the cell and therefore have diverse uptake rates. The dissimilar uptake by different cells might explain the higher reduction of proliferation of cells after exposure to 50 nm AuNPs treatment in A549 cells and the increase in proliferation observed in the CHOK1 cells after 50 nm AuNP treatment. However, more detailed investigations are necessary to determine subcellular events.

#### **4.4. Oxidative Stress**

Elevated ROS can result in mitochondrial and DNA damage causing program and accidental cell death (125). Therefore, the H2DCFDA fluorescent assay was used to determine the level of ROS production caused by AuNP.

30 nm treated CHOK1 cells (Figure 3.3.1) show a significant ( $P < 0.001$ ) increase in ROS production after both 4h and 24h exposure. Surprisingly, cells treated with 50nm revealed a significantly lower production in ROS after 4h compared to the control sample (Figure 3.3.1). This can be explained by cells being able to adapt to their environment and overcome the initial stages of shock when exposed to the AuNPs. Similarly, Wu *et al* (2011) showed that cells exposed to oxidative stress can either adapt or become injured (126). Oxidative stress is one of the main mechanisms of nanoparticle-induced cytotoxicity, particularly metallic nanoparticles like AuNPs (127). In cellular systems the evaluation of ROS by AuNPs has shown to cause numerous biological effects which lead to either apoptosis or necrosis. The exact mechanism between AuNPs and the production of ROS is not fully understood, however it is predicted that AuNP-induced oxidative stress occurs via the impairment in mitochondrial functions due to an increase in intracellular ROS levels (127). Literature has reported a dose-dependent increase in ROS levels elicited by 10-15 nm citrate AuNPs, this was associated with an increase in caspase 3 and 7 which lead to apoptosis by mitochondrial dysfunction (128).

The control set was not treated with AuNPs yet produced a higher ROS production in comparison to exposed samples. This could be explained that oxidative species are not only formed under pathological situations (various diseases) but even under non-pathological events such as cellular metabolism (126). Studies have shown that culture media containing serum may affect DCF fluorescence (129) thus in this study as seen in *section 2.5* serum reduced media was utilized but, even though the serum was reduced to 2% it could still have resulted in an increase in the fluorescent reading leading to the higher ROS production within the control sample. It has also been said that the fluorescent probe can be inefficient due to their ability to react with a variety of reactive species, causing misleading results (130).

All AuNP sizes after 24h showed a significant increase in ROS production. Additionally, an increase in ROS production was observed as the concentration of AuNPs increased. Similar results were found by Lee *et al* (2019), they concluded that the level of ROS correlates with the concentration. Exposure to high levels of AuNPs overwhelms the antioxidant system and results in cytotoxicity and inflammation. The concentration of ROS in cells can rise significantly, reaching the threshold that can trigger program cell death (116,131). As demonstrated by Mateo *et al* (2014) cell lines have different maximum ROS levels. The study showed that for HL-60 cell and HepG2 reached a maximum after 24h and 1h respectively (131). This could explain why after 24h treatment in CHOK1 cells all sizes revealed a significant ROS production. Overall, no noticeable differences were detected in ROS generation in the cells exposed to the different sized AuNPs. This was upheld by Mateo *et al* (2015) as they concluded that AuNP induced cytotoxicity mediated by oxidative stress is independent of the AuNP size (131).

For 30nm and 80nm AuNPs at 10 µg/ml, no significant effect on A549 cells were seen. However at the lowest and highest concentrations a significant increases in ROS levels were observed. A549 cells showed a significant ( $P < 0.001$ ) increase in ROS production after 24h exposure for 30nm, 50 nm and 80nm particles. Thus displaying similar results to that of CHOK1 cells where all AuNPs showed a substantial increase in ROS after 24h exposure at all concentrations. It is clearly seen from (Figure 3.3.2 I and J) that after 4h, 50nm resulted in the highest ROS production and after 24h, the 30nm particles displayed the highest ROS levels in the A549 cells. This is possibly due to oxidative stress and cytotoxicity of the AuNPs as it has been shown that AuNPs sometimes impair mitochondrial function. Taggart *et al* (2014) demonstrated that 1.9 nm AuNPs (500µg/ml) caused oxidation of the mitochondrial membrane protein, cardiolipin and cell specific disruption of mitochondrial membrane potential (132).

The oxidation of cardiolipin initiates the intrinsic apoptotic pathway, by releasing cytochrome c into the cytosol (133). Both human breast adenocarcinoma and T98G (human glioblastoma multiforma tumour) cells showed oxidation of cardiolipin in the presence of AuNPs. The effect of AuNPs on the mitochondria might be also directly related to DNA damage upon the exposure to AuNPs, as mitochondria have been shown to play a role in the induction of DNA damage (132).

#### **4.5. AuNP-induced Apoptosis**

The distribution and morphology of the cell's nucleus are indicators for cell cycle progression, it aids in distinguishing between cell types, mutation identification or changes induced by drugs (134). Apoptotic cells show changes in cell morphology characterised by condensation of chromatin, DNA cleavage, loss of cell volume, blebbing of plasma membrane and nuclear fragmentation (135). Having a compound-drug that has the ability to trigger apoptosis in cancerous cells is very desirable in cancer treatment. The effect of AuNPs on cell morphology and cell death was detected via fluorescent staining with Hoechst 33342 and acridine orange dye.

As seen in Figure 3.4.1 at 4h and 24h although apoptosis is present it is only to a small extent. Apoptosis or programmed cell death is an important process in the development of multicellular organisms (135) and is present even in the absence of insult. At 48h, cells were observed with orange/reddish staining surrounding the nucleus, this can be explained by AO acting as a fluorophore that accumulates in acidic vesicular organelles such as autolysosomes. The AO then dimerizes resulting in a metachromatic shift from green to red, this may then be measured for late-stage autophagy (135,136). Thus autophagy is observed at 30 nm AuNPs at 48h. Changes in cell density can be seen at 48h for 30 nm and 50 nm this may be indicative of the cytotoxic effect of AuNPs to long exposure periods. It can thus be concluded that for CHOK1 cells, AuNPs in this study did affect the cells on a cellular level (confirmed via WST-1, CV and ROS assay), but the cytotoxic effects cannot be ascribed to apoptosis induction. Similarly, A549 cells did not present much apoptosis. At 24h no apoptosis was observed, nuclei were all healthy and evenly fluorescent. Several researchers report that change in fluorescence (brighter) is typical of early apoptosis (89,137), and although this was present, a different type of cell death is possibly that cause of the decrease in proliferation observed in both cell lines. These results show that neither CHOK1 nor A549 cells had AuNP induced apoptosis. However, the application of a triple stain method using Hoechst, Acridine Orange and Propidium iodine may provide a better conclusion to the particular cell death.

## SUMMARY AND CONCLUSION

---

DLS and ZP analysis was conducted for validation of AuNP size and surface charge, respectively. DLS showed the expected increased  $R_H$  for both 30nm and 80 nm AuNPs. For 50 nm particles, the size decreased to 48.24 d.nm, this result could be explained by electrostatic effect also known as interparticle or intermolecular interactions (104). All sizes (30 nm, 50 nm and 80 nm) showed to be moderately polydispersed. All sizes are anionic and stable. The AuNPs were citrate coated and based on the characterization results was suitable to use in this particular investigation.

When investigating the impact of AuNPs on cellular proliferation 30 nm particles showed to be the most cytotoxic to CHO-K1 cells across all exposure times by resulting in a significant decrease in cell proliferation. On the contrary 50 nm particles caused a significant increase in proliferation after 4h exposure. This finding indicates that 50 nm particles are optimal for treatment in CHO-K1 cells as no cytotoxicity is induced. Conclusive results however cannot be made without further investigation and possibly more cytotoxic assays. It was evident that 48h exposure was too long for CHO-K1 cells across all sizes and all concentrations. Significant reduction in proliferation was observed. This shows that when treating CHO-K1 cells 48h may not be ideal and that shorter exposure times should be investigated. However, after 24h and 48h a dose-dependent effect was seen. A549 cells although not significant, showed an increase in cell proliferation after 4h incubation. 50 nm and 80 nm AuNPs at 15  $\mu\text{g/ml}$  had the most prominent effect on A549 cells across all time periods, at the highest concentration these sizes had a significant ( $P < 0.001$ ) decrease on cellular proliferation. As for 5 and 10  $\mu\text{g/ml}$  results varied across size and exposure times. This study showed that different cells display different sensitivity to AuNP treatment.

When observing cell viability by WST-1 results were conflicting for both CHO-K1 and A549 cells. For CHO-K1 cells treated with 30 nm AuNPs cytotoxicity was seen and this corresponds with the CV results. However, at 50 nm and 80 nm exposure results were contradictory, 50 nm after 4h did not display an increased viability but rather a decrease. With 80 nm AuNPs after 24 h, a significant increase in cell viability was seen with WST-1 but not the case with CV (cell proliferation). This was also observed in A549 cells, however WST-1 results coincides with CV that 50 nm and 80 nm AuNPs at 15  $\mu\text{g/ml}$  is cytotoxic. The conflicting results may be

explained *Bahadar et al* (2016) that cytotoxicity is dependent on the type of toxicity assay, cell line, physical and chemical properties (34).

The ROS production analysis showed that after 24h exposure significant increase in ROS levels were seen for all sizes at all concentrations for both CHO-K1 and A549. For CHO-K1 cells results for ROS production corresponded with that of CV. At 30 nm AuNPs for CHO-K1 cells, cells seem to adapt and decrease ROS levels after 24h. It is however clearly seen that 30 nm AuNPs induce oxidative stress whilst at 50 nm AuNPs the control sample produced a higher ROS level. For A549 results once again coincide with that of both cell proliferation and viability results. At 50 nm and 80 nm AuNP exposure 15 µg/ml produced significant ROS. Oxidative stress showed to be concentration-dependent for A549 cells.

The examination of cell death via dual staining showed that although morphological changes in nuclei were seen it was not enough to deduce it as AuNP-induced cell death. Thus for particular study AuNP effects were on a cellular level. However, additional staining methods should be employed to determine the exact type of cell death.

The study provided a baseline assessment showing that AuNP toxicity is size, concentration, cell-type and even time-dependent. This is one of the reasons why there are many contradiction in scientific literature on the cytotoxic effects of AuNPs. This study illustrates that conclusions should not be generalized as the results of *in vitro* will always differ depending on AuNP size, concentrations, incubation time and cell type under investigation. Therefore, a broader range of cell lines need to be evaluated with set parameters, conclusive results can then be made on particular cells with particular parameters. However, for this study it was seen that AuNPs have stimulatory effects on cell viability and proliferation in normal (non-cancerous) cells. It also showed significant oxidative stress in cancerous cells. It can thus be postulated that 50 nm AuNPs at 24 hours could be an optimal probe for radiosensitization analysis, as it stimulated non-cancerous cells (CHO-K1) whilst having a cytotoxic effect on cancerous cells (A549). These findings can thus be utilized to employ the optimal AuNP to be used as a radiosensitizing particle in cells. In the future, it might provide an opportunity to develop target specific treatment as AuNPs can be highly functionalized. This study contributes to the understanding of how AuNP effects change within different cell models and that there is still an extensive amount of *in vitro* and *in vivo* research required to fully understand the mechanism of AuNPs before any clinical applications.

Future Studies: Internalised citrate coated spherical AuNPs should be quantified via inductively coupled plasma atomic emission spectroscopy (ICP-AES) to explain different results found in ROS and viability assay and be further investigated for their radiosensitivity effect before used in clinical environment for radiotherapy. In addition, AuNPs can be investigated with respect to how it affects the cell cycle kinetics, using bromodeoyuridine (BrdU) proliferation and different cell death assays.



## REFERENCES

---

1. WHO. Latest global cancer data: Cancer burden rises to 18.1 million new cases and 9.6 million cancer deaths in 2018. *J Med Soc Toho Univ.* 2018;50(1):106–7.
2. Haume K, Rosa S, Grellet S, Śmiałek MA, Butterworth KT, Solov'yov A V., et al. Gold nanoparticles for cancer radiotherapy: a review. *Cancer Nanotechnol.* 2016;7(1).
3. Mehta SR, Suhag V, Semwal M, Sharma N. Radiotherapy: Basic concepts and recent advances. *Med J Armed Forces India [Internet].* 2010;66(2):158–62. Available from: [http://dx.doi.org/10.1016/S0377-1237\(10\)80132-7](http://dx.doi.org/10.1016/S0377-1237(10)80132-7)
4. Peng J, Liang X, Calderon L. Progress in research on gold nanoparticles in cancer management. *Med (United States).* 2019;98(18).
5. Apanasevich V, Avramenko V, Lukyanov P, Lagureva, A. Polkovnikova A, Lukyanenko K, Kustov V, et al. Enhance the absorption of gamma-ray energy inside the tumor using gold nanoparticles and iodine particles. *Cancer Oncol Res.* 2014;2(2):17–20.
6. Mordorski B, Landriscina A, Friedman A. An Overview of Nanomaterials in Dermatology. *Nanosci Dermatology [Internet].* 2016;31–46. Available from: <http://dx.doi.org/10.1016/B978-0-12-802926-8.00003-3>
7. Gaur A, Midha A, Bhatia A. Significance of nanotechnology in medical sciences. *Asian J Pharm.* 2008;2(2):80.
8. Li C, Li Z, Wang Y, Liu H. Gold Nanoparticles Promote Proliferation of Human Periodontal Ligament Stem Cells and Have Limited Effects on Cells Differentiation. *J Nanomater.* 2016;1–11.
9. Bell IR, Ives JA, Jonas WB. Nonlinear effects of nanoparticles: Biological variability from hormetic doses, small particle sizes, and dynamic adaptive interactions. *Int Dose-Response Soc.* 2014;12(2):202–32.
10. Verma HN, Singh P, Chavan RM. Gold nanoparticle: Synthesis and characterization. *Vet World.* 2014;7(2):72–7.
11. Herizchi R, Abbasi E, Milani M, Akbarzadeh A. Current methods for synthesis of gold nanoparticles. *Artif Cells, Nanomedicine Biotechnol.* 2016;44(2):596–602.

12. Frens G. Controlled Nucleation for the Regulation of the Particle Size in Monodisperse Gold Suspensions. *Nat Phys Sci.* 1973;241:20.
13. Cunningham A, Burgi T. Bottom-up Organisation of Metallic Nanoparticles. In: Rockstuhl C, Scharf T, editors. *Amorphous Nanophotonics.* Berlin, Heidelberg: Springer; 2013.
14. Shah M, Badwaik V, Kherde Y, Waghvani HK, Modi T, Aguilar ZP, et al. Gold nanoparticle: various methods of synthesis and antibacterial application. *Front Biosci.* 2014;19(8):1320–44.
15. Kimling J, Maier M, Okenve B, Kotaidis V, Ballot H, Plech A. Turkevich method for gold nanoparticle synthesis revisited. *J Phys Chem B.* 2006;110(32):15700–7.
16. Ji X, Song X, Li J, Bai Y, Yang W, Peng X. Size Control of Gold Nanocrystals in Citrate Reduction: The Third Role of Citrate. *J Am Chem Soc.* 2007;129(45):13939–48.
17. Kumar S, Gandhi K, Kumar R. Modeling of Formation of Gold Nanoparticles by Citrate Method. *Ind Eng Chem Res.* 2007;46(10):3128–36.
18. Li C, Li D, Wan G, Jie X, Wangou H. Facile synthesis of concentrated gold nanoparticles with low size-distribution in water: temperature and pH controls. *Nanoscale Res Lett* 6. 2011;440:1–10.
19. Verbeke D, Dierckx S, Dewettinck K. Exudate gums: Occurrence, production, and applications. *Appl Microbiol Biotechnol.* 2003;63(1):10–21.
20. Ribeiro De Barros H, Cardoso MB, Camargo De Oliveira C, Cavichiolo Franco CR, De Lima Belan D, Vidotti M, et al. Stability of gum Arabic-gold nanoparticles in physiological simulated pHs and their selective effect on cell lines. *RSC Adv.* 2016;6(12):9411–20.
21. Lead J, Wilkinson K. Aquatic Colloids and Nanoparticles : Current Knowledge and Future Trends. *EnvironChem.* 2006;3:159–71.
22. Hunt LB. The True Story of Purple of Cassius AND ENAMEL COLOURS. *Gold Bull.* 1976;9(4):134–9.
23. Dykman LA, Khlebtsov NG. Gold Nanoparticles in Biology and Medicine : Recent Advances and Prospects. *Acta Naturae.* 2011;3(9):34–55.

24. Faulk P, Taylor M. Communication to the editors: An immunocolloid method for the electron microscope. *Immunochemistry*. 1971;8(11):1081–3.
25. Sun H, Jia J, Jiang C, Zhai S. Gold nanoparticle-induced cell death and potential applications in nanomedicine. *Int J Mol Sci*. 2018;19(3):1–20.
26. Hutter E, Maysinger D. Gold nanoparticles and quantum dots for bioimaging. *Microsc Res Tech*. 2011;74(7):592–604.
27. Arvizo R, Bhattacharya R, Mukherjee P. Gold nanoparticles: Opportunities and challenges in nanomedicine. *Expert Opin Drug Deliv*. 2010;7(6):753–63.
28. Posch C, Latorre A, Crosby MB, Celli A, Latorre A, Vujic I, et al. Detection of GNAQ mutations and reduction of cell viability in uveal melanoma cells with functionalized gold nanoparticles. *Biomed Microdevices*. 2015;17(1).
29. Ajdari N, Vyas C, Bogan SL, Lwaleed BA, Cousins BG. Gold nanoparticle interactions in human blood: a model evaluation. *Nanomedicine Nanotechnology, Biol Med* [Internet]. 2017;13(4):1531–42. Available from: <http://dx.doi.org/10.1016/j.nano.2017.01.019>
30. Farokhzad OC, Langer R. *Impact of Nanotechnology on Drug Delivery*. ACS. 2009;3(1):16–20.
31. Couvreur P. Nanoparticles in drug delivery : Past , present and future ☆. *Adv Drug Deliv Rev* [Internet]. 2012;65(1):4–6. Available from: <http://dx.doi.org/10.1016/j.addr.2012.04.010>
32. Silva J, Fernandes AR, Baptista P V. Application of Nanotechnology in Drug Delivery. In: Sezer A, editor. *Application of Nanotechnology in Drug Delivery* [Internet]. Intech Open; 2014. p. 128–54. Available from: <https://www.intechopen.com/books/application-of-nanotechnology-in-drug-delivery/application-of-nanotechnology-in-drug-delivery>
33. Pan Y, Neuss S, Leifert A, Fischler M, Wen F, Simon U, et al. Size-Dependent Cytotoxicity of Gold Nanoparticles. *Small*. 2007;11:1941–9.
34. Bahadar H, Maqbool F, Niaz K, Abdollahi M. Toxicity of nanoparticles and an overview of current experimental models. *Iran Biomed J*. 2016;20(1):1–11.

35. Chueh PJ, Liang RY, Lee YH, Zeng ZM, Chuang SM. Differential cytotoxic effects of gold nanoparticles in different mammalian cell lines. *J Hazard Mater* [Internet]. 2014;264:303–12. Available from: <http://dx.doi.org/10.1016/j.jhazmat.2013.11.031>
36. Sukhanova A, Bozrova S, Sokolov P, Berestovoy M, Karaulov A, Nabiev I. Dependence of Nanoparticle Toxicity on Their Physical and Chemical Properties. *Nanoscale Res Lett*. 2018;13(44):1–21.
37. Connor EE, Mwamuka J, Gole A, Murphy CJ, Wyatt MD. Toxicity of nanoparticles Gold Nanoparticles Are Taken Up by Human Cells but Do Not Cause Acute Cytotoxicity. *Small*. 2005;1(3):325–7.
38. Goodman CM, Mccusker CD, Yilmaz T, Rotello VM. Toxicity of Gold Nanoparticles Functionalized with Cationic and Anionic Side Chains. *Bioconjugate Chem*. 2004;15:897–900.
39. Boisselier E, Astruc D. Gold nanoparticles in nanomedicine: preparations, imaging, diagnostics, therapies and toxicity. *Chem Soc Rev*. 2009;38(6):1759–82.
40. Patra HK, Banerjee S, Chaudhuri U, Lahiri P, Dasgupta AK. Cell selective response to gold nanoparticles. *Nanomedicine Nanotechnology, Biol Med*. 2007;3(2):111–9.
41. Vetten MA, Tlotleng N, Tanner Rascher D, Skepu A, Keter FK, Boodhia K, et al. Label-free in vitro toxicity and uptake assessment of citrate stabilised gold nanoparticles in three cell lines. *Part Fibre Toxicol* [Internet]. 2013;10(1):1. Available from: *Particle and Fibre Toxicology*
42. Mironava T, Hadjiargyrou M, Simon M, Jurukovski V, Rafailovich MH. Gold nanoparticles cellular toxicity and recovery: Effect of size, concentration and exposure time. *Nanotoxicology*. 2010;4(1):120–37.
43. Suh KS, Lee YS, Seo SH, Kim YS, Choi EM. Gold nanoparticles attenuates antimycin A-induced mitochondrial dysfunction in MC3T3-E1 osteoblastic cells. *Biol Trace Elem Res*. 2013;153(1–3):428–36.
44. Abdelhalim MAK, Jarrar BM. Gold nanoparticles induced cloudy swelling to hydropic degeneration , cytoplasmic hyaline necrosis in the liver. *Lipids Health Dis* [Internet]. 2011;10(1):166. Available from: <http://www.lipidworld.com/content/10/1/166>
45. Cho EC, Xie J, Wurm PA, Xia Y. Understanding the Role of Surface Charges in Cellular

- Adsorption versus Internalization by Selectively Removing Gold Nanoparticles on the Cell Surface with a I 2 / KI Etchant 2009. *Nano Lett.* 2009;9(3):1080–4.
46. Gratton SEA, Ropp PA, Pohlhaus PD, Luft JC, Madden VJ, Napier ME, et al. The effect of particle design on cellular internalization pathways. *Proc Natl Acad Sci U S A.* 2008;105(33):11613–8.
  47. Xia Q, Li H, Liu Y, Zhang S, Feng Q, Xiao K. The effect of particle size on the genotoxicity of gold nanoparticles. *J Biomed Mater Res - Part A.* 2017;105(3):710–9.
  48. Ishidate M, Miura KF, Sofuni T. Chromosome aberration assays in genetic toxicology testing in vitro. *Mutat Res - Fundam Mol Mech Mutagen.* 1998;404(1–2):167–72.
  49. Kwatra D, Venugopal A, Anant S. Nanoparticles in radiation therapy : a summary of various approaches to enhance radiosensitization in cancer. *Transl Cancer Res.* 2013;2(4):330–42.
  50. Rahman WN, Bishara N, Ackerly T, He CF, Jackson P, Wong C, et al. Enhancement of radiation effects by gold nanoparticles for superficial radiation therapy. *Nanomedicine Nanotechnology, Biol Med* [Internet]. 2009;5(2):136–42. Available from: <http://dx.doi.org/10.1016/j.nano.2009.01.014>
  51. Chithrani DB, Jelveh S, Jalali F, Prooijen M Van, Allen C, Bristow RG, et al. Gold Nanoparticles as Radiation Sensitizers in Cancer Therapy Gold Nanoparticles as Radiation Sensitizers in Cancer Therapy. *Radiat Res* [Internet]. 2010;173(6):719–28. Available from: url: <http://www.bioone.org/doi/full/10.1667/RR1984.1%0ABioOne>
  52. Roa W, Zhang X, Guo L, Shaw A, Hu X, Xiong Y, et al. Gold nanoparticle sensitize radiotherapy of prostate cancer cells by regulation of the cell cycle. *Nanotechnology.* 2009;20(375101):1–9.
  53. Coulter J, Jain S, Taggart LE, Dickson GR, McMahon SJ, Hyland WB, et al. Cell type-dependent uptake, localization, and cytotoxicity of 1.9 nm gold nanoparticles. *Int J Nanomedicine.* 2012;7:2673–85.
  54. Jain SJ, Coulter JA, Hounsell AR, Butterworth KT, McMahon SJ, Hyland WB, et al. Cell-Specific Radiosensitization By Gold Nanoparticles At Megavoltage Radiation Energies. *Int J Radiat Oncol Biol Phys.* 2011;79(2):531–9.
  55. Zhang Z, Berg A, Levanon H, Fessenden RW, Meisel D. On the Interactions of Free

- Radicals with Gold Nanoparticles. *J of Am Chem Soc.* 2003;125(26):7959–63.
56. Jiang WEN, Kim BYS, Rutka JT, Chan WCW. Nanoparticle-mediated cellular response is size-dependent. *Nat Nanotechnol.* 2008;3:145–50.
  57. Zhang BS, Li J, Lykotrafitis G, Bao G, Suresh S. Size-Dependent Endocytosis of Nanoparticles. *Av Mater.* 2009;23:419–24.
  58. Chithrani BD, Ghazani AA, Chan WCW. Determining the Size and Shape Dependence of Gold Nanoparticle Uptake into Mammalian Cells. *Nano Lett.* 2006;6(4):662–8.
  59. Conner SD, Schmid SL. Regulated portals of entry into the cell. *Nature* [Internet]. 2003;422(6927):37–44. Available from: <http://www.ncbi.nlm.nih.gov/pubmed/12621426>
  60. Doherty GJ, McMahon HT. Mechanisms of endocytosis. *Annu Rev Biochem* [Internet]. 2009;78:857–902. Available from: <http://www.ncbi.nlm.nih.gov/pubmed/19317650>
  61. Pucadyil TJ. Conserved Functions of Membrane Active GTPases in Coated Vesicle Formation. *Science* (80- ). 2010;1217(2009):1217–21.
  62. Chithrani DB. Nanoparticles for Improved Therapeutics and Imaging in Cancer Therapy. *Recent Pat Nanotechnol.* 2010;4:171–80.
  63. Chithrani BD, Chan WCW. Elucidating the Mechanism of Cellular Uptake and Removal of Protein-Coated Gold Nanoparticles of Different Sizes and Shapes. *Nano Lett.* 2007;7(6):1542–50.
  64. Leroueil PR, Berry SA, Duthie K, Han G, Rotello VM, Mcnerny DQ, et al. Wide Varieties of Cationic Nanoparticles Induce Defects in Supported Lipid Bilayers. *Nano Lett.* 2008;8(2):420–4.
  65. Muthu MS, Feng SS. Theranostic liposomes for cancer diagnosis and treatment: Current development and pre-clinical success. *Expert Opin Drug Deliv.* 2013;10(2):151–5.
  66. Goel R, Shah N, Visaria R, Paciotti GF, Bischof JC. Biodistribution of TNF- $\alpha$ -coated gold nanoparticles in an in vivo model system. *Nanomedicine.* 2009;4(4):401–10.
  67. Zhou C, Long M, Qin Y, Sun X, Zheng J. Luminescent Gold Nanoparticles with Efficient Renal Clearance. *Angew Chemie Int Ed.* 2011;50:3168–72.
  68. Chen H, Dorrigan A, Saad S, Hare DJ, Cortie MB, Valenzuela SM. In Vivo Study of

- Spherical Gold Nanoparticles: Inflammatory Effects and Distribution in Mice. *PLoS One*. 2013;8(2).
69. Chen YS, Hung YC, Liao I, Huang GS. Assessment of the in vivo toxicity of gold nanoparticles. *Nanoscale Res Lett*. 2009;4(8):858–64.
  70. Zhang X, Wu D, Shen X, Liu P, Fan F, Fan S. In vivo clearance, biodistribution, toxicity of gold nanoclusters. *Biomaterials*. 2012;33:4628–38.
  71. Cho WS, Kim S, Han BS, Son WC, Jeong J. Comparison of gene expression profiles in mice liver following intravenous injection of 4 and 100 nm-sized PEG-coated gold nanoparticles. *Toxicol Lett*. 2009;191(1):96–102.
  72. Lasagna-Reeves C, Gonzalez-Romero D, Barria MA, Olmedo I, Clos A, Sadagopa Ramanujam VM, et al. Bioaccumulation and toxicity of gold nanoparticles after repeated administration in mice. *Biochem Biophys Res Commun* [Internet]. 2010;393(4):649–55. Available from: <http://dx.doi.org/10.1016/j.bbrc.2010.02.046>
  73. Kim JH, Kim JH, Kim KW, Kim MH, Yu YS. Intravenously administered gold nanoparticles pass through the blood-retinal barrier depending on the particle size, and induce no retinal toxicity. *Nanotechnology*. 2009;20(50):1–8.
  74. Sadauskas E, Danscher G, Stoltenberg M, Vogel U, Larsen A, Wallin H. Protracted elimination of gold nanoparticles from mouse liver. *Nanomedicine Nanotechnology, Biol Med* [Internet]. 2009;5(2):162–9. Available from: <http://dx.doi.org/10.1016/j.nano.2008.11.002>
  75. Balasubramanian SK, Jittiwat J, Manikandan J, Ong CN, Yu LE, Ong WY. Biodistribution of gold nanoparticles and gene expression changes in the liver and spleen after intravenous administration in rats. *Biomaterials* [Internet]. 2010;31(8):2034–42. Available from: <http://dx.doi.org/10.1016/j.biomaterials.2009.11.079>
  76. Cho WS, Cho M, Jeong J, Choi M, Cho HY, Han BS, et al. Acute toxicity and pharmacokinetics of 13 nm-sized PEG-coated gold nanoparticles. *Toxicol Appl Pharmacol*. 2009;236(1):16–24.
  77. Lopez-Chaves C, Soto-Alvaredo J, Montes-Bayon M, Bettmer J, Llopis J, Sanchez-Gonzalez C. Gold nanoparticles: Distribution, bioaccumulation and toxicity. In vitro and in vivo studies. *Nanomedicine Nanotechnology, Biol Med* [Internet]. 2018;14(1):1–12.

Available from: <https://doi.org/10.1016/j.nano.2017.08.011>

78. Bhattacharjee S. Review article DLS and zeta potential – What they are and what they are not? *J Control Release* [Internet]. 2016;235:337–51. Available from: <http://dx.doi.org/10.1016/j.jconrel.2016.06.017>
79. Jitkang L, Pin YS, Xin CH, Chun LS. Characterization of magnetic nanoparticle by dynamic light scattering. *Nanoscale Res Lett* [Internet]. 2013;8(1):308–81. Available from: [www.nanoscalereslett.com/content/8/1/381](http://www.nanoscalereslett.com/content/8/1/381)
80. Mudalige T, Qu H, Van Haute D, Ansar SM, Paredes A, Ingle T. Characterization of Nanomaterials: Tools and Challenges. In: *Nanomaterials for Food Applications* [Internet]. Elsevier Inc.; 2018. p. 313–53. Available from: <http://dx.doi.org/10.1016/B978-0-12-814130-4.00011-7>
81. May S, Hirsch C, Rippl A, Bohmer N, Kaiser JP, Diener L, et al. Transient DNA damage following exposure to gold nanoparticles. *Nanoscale*. 2018;10(33):15723–35.
82. Aslantürk ÖS. In Vitro Cytotoxicity and Cell Viability Assays : Disadvantages In Vitro Cytotoxicity and Viability Assays : Principles , Advantages , and Disadvantages. In: *Genotoxicity - A Predictable Risk to Our Actual World*. 2018. p. 2–17.
83. Vega-avila E, Pugsley MK. An overview of colorimetric assay methods used to assess survival or proliferation of mammalian cells An Overview of Colorimetric Assay Methods Used to Assess Survival or Proliferation of Mammalian Cells. 2011;(January).
84. Aslantürk ÖS. In Vitro Cytotoxicity and Cell Viability Assays: Principles, Advantages, and Disadvantages. *Genotoxicity - A Predict Risk to Our Actual World*. 2018;1–18.
85. Kalyanaraman B, Darley-usmar V, Davies KJA, Dennery PA, Jay H, Grisham MB, et al. Free Radical Biology & Medicine Measuring reactive oxygen and nitrogen species with fluorescent probes : challenges and limitations. *Free Radic Biol Med* [Internet]. 2012;52(1):1–6. Available from: <http://dx.doi.org/10.1016/j.freeradbiomed.2011.09.030>
86. Heng BC, Zhao X, Tan EC, Khamis N, Assodani A, Xiong S, et al. Evaluation of the cytotoxic and inflammatory potential of differentially shaped zinc oxide nanoparticles. *Arch Toxicol*. 2011;85(12):1517–28.
87. Pujalté I, Passagne I, Brouillaud B, Tréguer M, Durand E, Ohayon-Courtès C, et al.

- Cytotoxicity and oxidative stress induced by different metallic nanoparticles on human kidney cells. *Part Fibre Toxicol* [Internet]. 2011;8(1):10. Available from: <http://www.particleandfibretoxicology.com/content/8/1/10>
88. Ganesh R, Smeraldi J, Hosseini T, Khatib L, Olson BH, Rosso D. Evaluation of nanocopper removal and toxicity in municipal wastewaters. *Environ Sci Technol*. 2010;44(20):7808–13.
  89. Crowley LC, Marfell BJ, Waterhouse NJ. Analyzing cell death by nuclear staining with Hoechst 33342. *Cold Spring Harb Protoc*. 2016;(9):778–81.
  90. Digman M, Gratton E. Lessons in fluctuation correlation spectroscopy. *Annu Rev Phys Chem*. 2011;62:645–68.
  91. Kaszuba M, Corbett J, Watson FMN, Jones A. High-concentration zeta potential measurements using light-scattering techniques. *Philos Trans R Soc A Math Phys Eng Sci*. 2010;368(1927):4439–51.
  92. Kusuzaki K, Murata H, Takeshita H, Hashiguchi S, Nozaki T, Emoto K, et al. Intracellular binding sites of acridine orange in living osteosarcoma cells. *Anticancer Res*. 2000;20(2):971–5.
  93. Newhauser WD, Zhang R. The physics of proton therapy. *Phys Med Biol* [Internet]. 2015;60:R155–209. Available from: <http://dx.doi.org/10.1088/0031-9155/60/8/R155>
  94. Su S, Liu Q, Chen J, Chen J, Chen F, He C, et al. A Positive feedback loop between mesenchymal-like cancer cells and macrophages is essential to breast cancer metastasis. *Cancer Cell* [Internet]. 2014;25(5):605–20. Available from: <http://dx.doi.org/10.1016/j.ccr.2014.03.021>
  95. Patil M, Metha D, Guvva S. Future impact of nanotechnology on medicine and dentistry. *J Indian Soc Periodontol*. 2008;12(2):1–34.
  96. Sztandera K, Gorzkiewicz M, Klajnert-Maculewicz B. Gold Nanoparticles in Cancer Treatment. *Mol Pharm*. 2018;16(1):1–23.
  97. Zhang X, Wu D, Shen X, Chen J, Sun Y, Liu P, et al. Size-dependent radiosensitization of PEG-coated gold nanoparticles for cancer radiation therapy. *Biomaterials*. 2012;33:6408–19.

98. Chen M, Qiao G, Hylander BL, Mohammadpour H, Wang XY, Subjeck JR, et al. Adrenergic stress constrains the development of anti-tumor immunity and abscopal responses following local radiation. *Nat Commun* [Internet]. 2020;11(1). Available from: <http://dx.doi.org/10.1038/s41467-020-15676-0>
99. Penninckx S, Heuskin AC, Michiels C, Lucas S. Gold nanoparticles as a potent radiosensitizer: A transdisciplinary approach from physics to patient. *Cancers (Basel)*. 2020;12(8):1–361.
100. Zhou J, Ralston J, Sedev R, Beattie DA. Functionalized gold nanoparticles: Synthesis, structure and colloid stability. *J Colloid Interface Sci* [Internet]. 2009;331(2):251–62. Available from: <http://dx.doi.org/10.1016/j.jcis.2008.12.002>
101. Park JW, Shumaker-Parry JS. Structural study of citrate layers on gold nanoparticles: Role of intermolecular interactions in stabilizing nanoparticles. *J Am Chem Soc*. 2014;136(5):1907–21.
102. Liu W, Rose J, Plantevin S, Auffan M, Bottero J-Y, Vidaud C. Protein corona formation for nano materials and proteins of a similar size: hard or soft corona? *Nanoscale*. 2013;5:1658–68.
103. Milani S, Bombelli FB, Pitek AS, Dawson KA. Reversible versus Irreversible Binding of Transferrin to Polystyrene Nanoparticles : Soft and Hard Corona. *ACS Nano*. 2012;6(3):2532–41.
104. Nobbmann U. Why does DLS say that my particles are too small? [Internet]. Malvern Panalytical. 2016. p. 1–2. Available from: <https://www.materials-talks.com/blog/2016/08/16/why-does-dls-say-that-my-particles-are-too-small/>
105. Danaei M, Dehghankhold M, Ataei S, Davarani FH, Javanmard R, Dokhani A, et al. Impact of Particle Size and Polydispersity Index on the Clinical Applications of Lipidic Nanocarrier Systems. *Pharmaceutics*. 2018;10(57):1–17.
106. Vechia IC Della, Steiner BT, Freitas ML, Fidelis G dos SP, Galvani NC, Ronchi JM, et al. Comparative cytotoxic effect of citrate-capped gold nanoparticles with different sizes on noncancerous and cancerous cell lines. *J Nanopart Res*. 2020;22(133):1–11.
107. Kapara A, Brunton V, Graham D, Faulds K. Investigation of cellular uptake mechanism of functionalised gold nanoparticles into breast cancer using SERS. *Chem Sci*.

- 2020;11(22):5819–29.
108. Fröhlich E. The role of surface charge in cellular uptake and cytotoxicity of medical nanoparticles. *Int J Nanomedicine*. 2012;7:5577–91.
  109. Honary S, Zahir F. Effect of Zeta Potential on the Properties of Nano-Drug Delivery Systems - A Review (Part 1). *Trop J Pharm Res*. 2013;12(2):255–64.
  110. Alkilany AM, Murphy CJ. Toxicity and cellular uptake of gold nanoparticles : what we have learned so far ? *J Nanoparticle Researfch*. 2010;12:2313–33.
  111. Vesaratchanon S, Nikolov A, Wasan DT. Sedimentation in nano-colloidal dispersions: Effects of collective interactions and particle charge. *Adv Colloid Interface Sci*. 2007;134–135:268–78.
  112. Wang W, Ding X, Xu Q, Wang J, Wang L, Lou X. Zeta-potential data reliability of gold nanoparticle biomolecular conjugates and its application in sensitive quantification of surface absorbed protein. *Colloids Surfaces B Biointerfaces* [Internet]. 2016;148:541–8. Available from: <http://dx.doi.org/10.1016/j.colsurfb.2016.09.021>
  113. Freese C, Gibson MI, Klok HA, Unger RE, Kirkpatrick CJ. Size- and coating-dependent uptake of polymer-coated gold nanoparticles in primary human dermal microvascular endothelial cells. *Biomacromolecules*. 2012;13(5):1533–43.
  114. Vijayakumar S, Ganesan S. In vitro cytotoxicity assay on gold nanoparticles with different stabilizing agents. *J Nanomater*. 2012;9(23):1–9.
  115. Goodman CM, Mccusker CD, Yilmaz T, Rotello VM. Toxicity of Gold Nanoparticles Functionalized with Cationic and Anionic Side Chains. *Bioconjugate Chem*. 2004;15:897–900.
  116. Lee YJ, Ahn EY, Park Y. Shape-dependent cytotoxicity and cellular uptake of gold nanoparticles synthesized using green tea extract. *Nanoscale Res Lett*. 2019;14:1–14.
  117. Champion JA, Katare YK, Mitragotri S. Particle shape: A new design parameter for micro- and nanoscale drug delivery carriers. *J Control Release*. 2007;121(1–2):3–9.
  118. Coradeghini R, Gioria S, García CP, Nativo P, Franchini F, Gilliland D, et al. Article in press. *Toxicol Lett*. 2013;217(3):1–12.
  119. Yue J, Feliciano TJ, Li W, Lee A, Odom TW. Gold nanoparticle size and shape effects

- on cellular uptake and intracellular distribution of siRNA nanoconstructs. *Bioconjugate Chem.* 2018;28(6):1791–800.
120. Lu S, Xia D, Huang G, Jing H, Wang Y, Gu H. Concentration effect of gold nanoparticles on proliferation of keratinocytes. *Colloids Surfaces B Biointerfaces* [Internet]. 2010;81(2):406–11. Available from: <http://dx.doi.org/10.1016/j.colsurfb.2010.06.019>
121. Cui W, Li J, Zhang Y, Rong H, Lu W, Jiang L. Effects of aggregation and the surface properties of gold nanoparticles on cytotoxicity and cell growth. *Nanomedicine Nanotechnology, Biol Med* [Internet]. 2012;8(1):46–53. Available from: <http://dx.doi.org/10.1016/j.nano.2011.05.005>
122. Liu Z, Wu Y, Guo Z, Liu Y, Shen Y, Zhou P, et al. Effects of Internalized Gold Nanoparticles with Respect to Cytotoxicity and Invasion Activity in Lung Cancer Cells. *PLoS One.* 2014;9(6):1–11.
123. Sun B, Hu N, Han L, Pi Y, Gao Y, Chen K. Anticancer activity of green synthesised gold nanoparticles from *Marsdenia tenacissima* inhibits A549 cell proliferation through the apoptotic pathway. *Artif Cells, Nanomedicine, Biotechnol* [Internet]. 2019;47(1):4012–9. Available from: <https://doi.org/10.1080/21691401.2019.1575844>
124. Rosli NS, Rahman AA, Aziz AA, Shamsuddin S. Determining the Size and Concentration Dependence of Gold Nanoparticles in Vitro Cytotoxicity ( IC 50 ) Test using WST-1 Assay. *Am Inst Phys Natl Phys Conf (PERFIK 2014).* 2015;1–5.
125. Minai L, Yeheskely-hayon D, Yelin D. following femtosecond pulse irradiation. *Sci Rep.* 2013;3(2146):1–7.
126. Wu D, Yotnda P. Production and Detection of Reactive Oxygen Species ( ROS ) in Cancers. *J Vis Exp.* 2011;57(e3357):1–4.
127. Her S, Jaffray DA, Allen C. Gold nanoparticles for applications in cancer radiotherapy: Mechanisms and recent advancements. *Adv Drug Deliv Rev* [Internet]. 2017;109:84–101. Available from: <http://dx.doi.org/10.1016/j.addr.2015.12.012>
128. Wahab R, Dwivedi S, Khan F, Mishra YK, Hwang IH, Shin HS, et al. Statistical analysis of gold nanoparticle-induced oxidative stress and apoptosis in myoblast (C2C12) cells.

- Colloids Surfaces B Biointerfaces [Internet]. 2014;123:664–72. Available from: <http://dx.doi.org/10.1016/j.colsurfb.2014.10.012>
129. Tetz LM, Kamau PW, Cheng AA, Meeker JD, Loch-Carusio R. Troubleshooting the dichlorofluorescein assay to avoid artifacts in measurement of toxicant-stimulated cellular production of reactive oxidant species. *Pharmacol Toxicol Methods*. 2013;67(2):56–60.
  130. Kumar V, Sharma N. In vitro and in vivo toxicity assessment of nanoparticles. *Int Nano Lett [Internet]*. 2017;7(4):243–56. Available from: <https://doi.org/10.1007/s40089-017-0221-3>
  131. Mateo D, Morales P, Avalos A, Haza AI. Oxidative stress contributes to gold nanoparticle-induced cytotoxicity in human tumor cells. *Toxicol Mech Methods*. 2014;24(3):161–72.
  132. Taggart LE, McMahon SJ, Currell FJ, Prise KM, Butterworth KT. The role of mitochondrial function in gold nanoparticle mediated radiosensitisation. *Cancer Nanotechnol*. 2014;5(5):1–12.
  133. Kagan VE, Tyurin VA, Jiang J, Tyurina YY, Ritov VB, Amoscato AA, et al. Cytochrome C Acts As A Cardiolipin Oxygenase Required for Release of Proapoptotic Factors. *Nat Chem Biol*. 2005;1(4):223–32.
  134. Bucevičius J, Lukinavicius G, Gerasimaite R. The Use of Hoechst Dyes for DNA Staining and Beyond. *Chemosensors*. 2018;6(18):1–12.
  135. Mpoke SS, Wolfe J. Differential staining of apoptotic nuclei in living cells: Application to macronuclear elimination in *Tetrahymena*. *J Histochem Cytochem*. 1997;45(5):675–83.
  136. Senthilkumar G, Skiba J, Kimple R. High-throughput quantitative detection of basal autophagy and autophagic flux using image cytometry. *Biotechniques*. 2019;67(2):70–3.
  137. Syed Abdul Rahman SN, Abdul Wahab N, Abd Malek SN. In vitro morphological assessment of apoptosis induced by antiproliferative constituents from the rhizomes of *curcuma zedoaria*. *Evidence-based Complement Altern Med*. 2013;2013.